Hindawi Publishing Corporation
Advances in Materials Science and Engineering
Volume 2016, Article ID 1509384, 19 pages
http://dx.doi.org/10.1155/2016/1509384

Research Article

Bifurcation Study of Thin Plate with an All-Over Breathing Crack

Lihua Chen, Jian Xue, Zhijie Zhang, and Wei Zhang

Beijing University of Technology, No. 100, Pingleyuan, Chaoyang District, Beijing, China

Correspondence should be addressed to Lihua Chen; chenlihua@bjut.edu.cn

Received 17 June 2016; Revised 17 September 2016; Accepted 16 October 2016

Academic Editor: Ying Li

An all-over breathing crack on the plate surface having arbitrary depth and location is assumed to be nonpropagating and parallel to one side of the plate. Based on a piecewise model, the nonlinear dynamic behaviors of thin plate with the all-over breathing crack are studied to analyze the effect of external excitation amplitudes and frequencies on cracked plate with different crack parameters (crack depth and crack location). Firstly, the mode shape functions of cracked thin plate are obtained by using the simply supported boundary conditions and the boundary conditions along the crack line. Then, natural frequencies and mode functions of the cracked plate are calculated, which are assessed with FEM results. The stress functions of thin plate with large deflection are obtained by the equations of compatibility in the status of opening and closing of crack, respectively. To compare with the effect of breathing crack on the plate, the nonlinear dynamic responses of open-crack plate and intact plate are analyzed too. Lastly, the waveforms, bifurcation diagrams, and phase portraits of the model are gained by the Runge-Kutta method. It is found that complex nonlinear dynamic behaviors, such as quasi-periodic motion, bifurcation, and chaotic motion, appear in the breathing crack plate.

1. Introduction

The plate is widely used in engineering practices such as the aircraft structure and body, concrete floor slabs, and marine industry, to name a few. The existence of a crack in a plate affects its stiffness, mass, and damping properties and then changes its vibration characteristics. For a vibration plate, a crack not only effects the free vibration of plate, including natural frequency and mode shape, but also changes the forced vibration, especially the response of nonlinear dynamics. The decrease of stiffness increases the vibration amplitude of the cracked plate with large deflection. Furthermore, the crack alternately opens and closes during vibration cycle, which forms the cracked structure with nonsmooth characteristics. Then, complex nonlinear dynamics behaviors will appear, which can seriously affect the safety of structures.

An earlier extensive literature review on the vibration of cracked structures could be found in the paper of Dimarogonas [1] in 1996. Rice and Levy [2] developed a line-spring model for approximate solution of a plate containing a part-through crack in 1972. Numerical results for natural frequencies of both isotropic and orthotropic plates with internal cracks were presented using subdomain method by Lee et al. [3]. Khadem and Rezaee [4] developed an analytical approach for crack detection in rectangular thin plates with an all-over part-through crack and subjected to uniform external loads using vibration analysis. Khadem and Rezaee [5] employed the modified comparison functions to obtain the natural frequencies of a simply supported rectangular cracked plate using the Rayleigh-Ritz method. Based on Mindlin plate theory (MPT), Hosseini-Hashemi et al. [6] proposed a set of exact closed-form characteristic equations to analyze free vibration problem of moderately thick rectangular plates with an arbitrary number of all-over part-through cracks.

For the nonlinear dynamic investigation of crack structures, many researchers considered cracks as open-crack models. In 2005, Fu et al. [7] derived the nonlinear equations of motion for the moderate thickness rectangular plates with transverse surface penetrating crack on the two-parameter foundation and analyzed the nonlinear vibration behaviors of the plate with different crack parameters. In 2009, Israr and Atepor [8] investigated nonlinear vibration of an isotropic cracked plate subjected to transverse harmonic excitation, both analytically and experimentally. In the same year,

Yang et al. [9] established nonlinear governing equations of motion for the simply supported functionally graded rectangular plate with a through-width surface crack to investigate the influences of material property gradient, crack depth, crack location, and plate thickness ratio on the vibration frequencies and transient response of the surface-racked FGM plate. Saito et al. [10] investigated veering phenomena in the nonlinear vibration frequencies of a cantilevered cracked plate and proposed an efficient method for estimating these frequencies. In 2012, Ismail and Cartmell [11] presented the forced vibration analysis of a plate with an inclined surface crack based on the classical plate theory. They formulated the inclined surface crack using a simplified line-spring model and utilized the multiple scale perturbation method to derive the amplitude-frequency equation of the cracked plate. In 2013, Bose and Mohanty [12] studied the vibration of a rectangular thin isotropic plate with a part-through surface crack of arbitrary orientation and position by using the Kirchhoff plate theory, and the problem of [11] was reconsidered and rigorously modified. AsadiGorgi et al. [13] investigated the flutter, limit cycle oscillation, and different nonlinear oscillations of rectangular panels with an all-over part-through crack in 2015. They performed these analyses for panels according to the first-order shear deformation or Mindlin plate theory and accurately studied the effects of the depths and locations of cracks on various aeroelastic characteristics of moderately thick rectangular panels.

In addition to the open crack, the surface crack breathing is a more practical and common situation during the vibration of the cracked structures [14]. The crack will stay open during one part of the vibration cycle and closed during the rest of the cycle which is usually called breathing.

In 2000, Pugno et al. [15] presented a technique capable of evaluating the dynamic response of a beam with several breathing cracks, which was based on the assumption of periodic response and the fact that cracks open and close continuously. The vibrational response to harmonic force of a cantilever beam with cracks of different sizes and locations was analyzed using this "harmonic balance" approach. In 2010, Caddemi et al. [16] investigated nonlinear dynamic response of beam with some switching cracks. They regarded the overall behavior of a beam with switching cracks as a sequence of linear phases, each of them characterised by different number and positions of the cracks in open state, and investigated the behavior under different boundary conditions for both harmonic loading and free vibrations. In 2016, Dotti et al. [17] studied the nonlinear dynamic response to simple harmonic excitation of a thin-walled beam with a breathing crack by employing a refined one-dimensional model.

The mentioned researches show that breathing crack model could reveal the real nonlinear dynamic behaviors of surface crack structures. Most of the researches on the crack of breathing are focused on the beam, and the nonlinear dynamics study of plate with surface crack employed the open-crack model.

The aim of this paper is to study the bifurcations of thin plate with an all-over breathing crack. The piecewise model is used to describe the opening and closing of breathing crack during the vibration: the crack is taken as open crack when crack opens; otherwise, the cracked plate is regarded as intact plate when crack closes. Based on the von Kármán large deflection theory, Hamilton's principle is used to establish the nonlinear governing equations of motion for the cracked plate. The mode shape functions are derived using the geometric boundary conditions and the boundary conditions along the crack line of thin plate. The effect of location and depth of crack on mode shapes and free vibration frequencies of cracked plate are analyzed, which is assessed with FEM results. The stress functions of cracked and intact plate with large deflection are obtained by the equations of compatibility. The partial differential equation is discretized via the Galerkin method. The Runge-Kutta method is utilized to investigate the bifurcations and chaotic motions of cracked plate. Nonlinear dynamic behaviors of cracked plate are studied to analyze the effect of external excitation amplitudes and frequencies on plate with different crack parameters which consist of crack depth and crack location.

2. Modal Analysis

In this section, the mode shape functions of cracked thin plate are obtained by using the simply supported boundary conditions and internal boundary conditions along the crack.

The simply supported rectangular plate with an all-over breathing crack can be illustrated by Figure 1. The thickness of the plate is H. The dimensions in x and y direction are a and b, respectively. Assume that (u_0, v_0, w_0) represent the displacements of a point in a mid-plane. The displacements of arbitrary point in the cracked plate are obtained as

$$u(x,y,z,t) = u_0(x,y,t) - z\frac{\partial w_0}{\partial x}, \tag{1a}$$

$$v(x,y,z,t) = v_0(x,y,t) - z\frac{\partial w_0}{\partial y}, \tag{1b}$$

$$w(x,y,z,t) = w_0(x,y,t). \tag{1c}$$

Using the Hamilton theory ($\int_0^T (\delta U + \delta V - \delta K)dt = 0$) and the von Karman large deflection theory, the nonlinear dynamic equations of the thin plate with large deflection are gained [18]:

$$\frac{\partial N_x}{\partial x} + \frac{\partial N_{xy}}{\partial y} = I_0\frac{\partial^2 u_0}{\partial t^2}, \tag{2a}$$

$$\frac{\partial N_{xy}}{\partial x} + \frac{\partial N_y}{\partial y} = I_0\frac{\partial^2 v_0}{\partial t^2}, \tag{2b}$$

$$\frac{\partial^2 M_x}{\partial x^2} + 2\frac{\partial^2 M_{xy}}{\partial x\partial y} + \frac{\partial^2 M_y}{\partial y^2} + N(w) + P = I_0\frac{\partial^2 w}{\partial t^2}, \tag{2c}$$

where $I_0 = \rho H$. The quantities (N_x, N_y, N_{xy}) are the in-plane force resultants, and (M_x, M_y, M_{xy}) are the moment

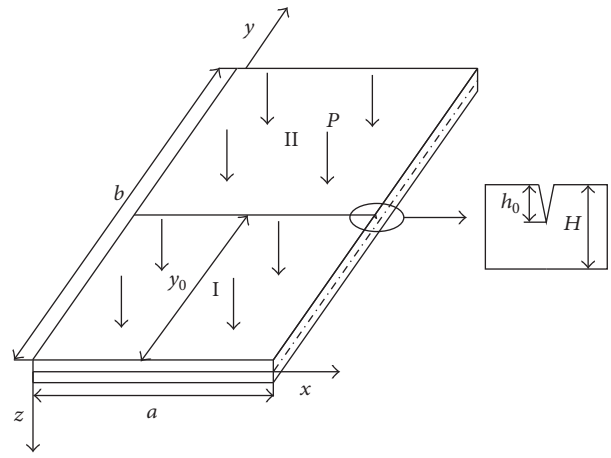

Figure 1: A simply supported rectangular thin plate with and all-over breathing crack.

resultants. P is external uniform load in the z direction. The expression $N(w_0)$ is as follows:

$$N(w) = \frac{\partial}{\partial x}\left(N_x\frac{\partial w}{\partial x} + N_{xy}\frac{\partial w}{\partial y}\right) + \frac{\partial}{\partial y}\left(N_{xy}\frac{\partial w}{\partial x} + N_y\frac{\partial w}{\partial y}\right). \tag{2d}$$

For the convenience of solving dynamic equations, a stress function $\varphi(x, y, t)$ is introduced to eliminate the in-plane displacements (u_0, v_0), and its relations with internal forces are obtained as

$$N_x = H\frac{\partial^2\varphi}{\partial y^2}, \tag{3a}$$

$$N_y = H\frac{\partial^2\varphi}{\partial x^2}, \tag{3b}$$

$$N_{xy} = -\frac{\partial^2\varphi}{\partial x\partial y}H. \tag{3c}$$

The compatibility equation in the form of stress function and transverse displacement is received:

$$\frac{\partial^4\varphi}{\partial x^4} + 2\frac{\partial^4\varphi}{\partial x^2\partial y^2} + \frac{\partial^4\varphi}{\partial y^4} = E\left[\left(\frac{\partial^2 w}{\partial x\partial y}\right)^2 - \frac{\partial^2 w}{\partial x^2}\frac{\partial^2 w}{\partial y^2}\right]. \tag{4}$$

Substituting (3a), (3b), and (3c) into the nonlinear dynamic equations (2a), (2b), (2c), and (2d), (2a) and (2b) will automatically meet balance conditions after ignoring the inertia terms. The dynamic equation of the stress function and deflection for (2c) is obtained as

$$-D\left(\frac{\partial^4 w}{\partial x^4} + 2\frac{\partial^4 w}{\partial x^2\partial y^2} + \frac{\partial^4 w}{\partial y^4}\right) + H\left(\frac{\partial^2\varphi}{\partial x^2}\frac{\partial^2 w}{\partial y^2} + \frac{\partial^2\varphi}{\partial y^2}\frac{\partial^2 w}{\partial x^2} - 2\frac{\partial^2\varphi}{\partial x\partial y}\frac{\partial^2 w}{\partial x\partial y}\right) + P = I_0\frac{\partial^2 w}{\partial t^2}. \tag{5}$$

The simply supported boundary conditions will be

$$x = 0 \text{ or } a: \quad u_0 = 0,\ w = 0,\ M_x = 0,\ N_{xy} = 0 \tag{6a}$$

$$y = 0 \text{ or } b: \quad v_0 = 0,\ w = 0,\ M_y = 0,\ N_{xy} = 0. \tag{6b}$$

In order to enable the boundary conditions to be expressed in terms of the stress function, $u_0 = 0$ and $v_0 = 0$ are substituted by $\Delta_u = 0$ and $\Delta_v = 0$, where [19]

$$\Delta_u = -\frac{1}{ab}\cdot\int_0^b\int_0^a\left[\frac{1}{E}\left(\frac{\partial^2\varphi}{\partial y^2} - \mu\frac{\partial^2\varphi}{\partial x^2}\right) - \frac{1}{2}\left(\frac{\partial w}{\partial x}\right)^2\right]dx\,dy, \tag{7a}$$

$$\Delta_v = -\frac{1}{ab}\cdot\int_0^b\int_0^a\left[\frac{1}{E}\left(\frac{\partial^2\varphi}{\partial x^2} - \mu\frac{\partial^2\varphi}{\partial y^2}\right) - \frac{1}{2}\left(\frac{\partial w}{\partial y}\right)^2\right]dx\,dy. \tag{7b}$$

As to the thin plate with an all-over crack, the authors divide the thin plate into two parts, plate I and plate II, at the location $y = y_0$, as shown in Figure 1.

Breathing crack is continuously open-closed during vibration. When the crack is open, at the crack location, the continuity and discontinuity conditions can be written along the crack line as follows:

$$w^{\mathrm{I}} = w^{\mathrm{II}}, \tag{8a}$$

$$u_0^{\mathrm{I}} = u_0^{\mathrm{II}}, \tag{8b}$$

$$v_0^{\mathrm{I}} = v_0^{\mathrm{II}}, \tag{8c}$$

$$M_y^{\mathrm{I}} = M_y^{\mathrm{II}}, \tag{8d}$$

$$V_y^{\mathrm{I}} = V_y^{\mathrm{II}}, \tag{8e}$$

$$N_y^{\mathrm{I}} = N_y^{\mathrm{II}}, \tag{8f}$$

$$N_{xy}^{\mathrm{I}} = N_{xy}^{\mathrm{II}}, \tag{8g}$$

$$\frac{\partial w^{\mathrm{I}}}{\partial y} - \frac{\partial w^{\mathrm{II}}}{\partial y} = \theta, \tag{8h}$$

where (8a)~(8g) represent displacement (w, u_0, v_0) and internal forces (M_y, V_y, N_y, N_{xy}) are equal on both sides of the crack, respectively. Equation (8h) represents the discontinuity condition of rotation angle along the crack. A line-spring model is used to describe the elastic behavior of the crack. θ is the rotation due to the presence of the crack and can be expressed as

$$\theta = \frac{12\left(1-\upsilon^2\right)}{E} \cdot \sigma_b \cdot \alpha_{bb}, \tag{9}$$

where σ_b is the nominal stress at a point far from the crack and α_{bb} is the dimensionless bending compliance factor. σ_b and α_{bb} are given by

$$\sigma_b = 6\frac{M_y}{H^2}, \tag{10a}$$

$$\alpha_{bb} = \frac{1}{H}\int_0^{h_0} g_b^2 dh, \tag{10b}$$

where g_b are dimensionless compliance coefficients, depending on the crack depth to thickness ratio $\xi = h_0/H$, and defined by [2]

$$g_b = \sqrt{\xi}\left(1.99 - 2.47\xi + 12.97\xi^2 - 23.11\xi^3 + 24.80\xi^4\right). \tag{11}$$

The mode shape functions for w of cracked thin plate are obtained by using the simply supported boundary conditions and the boundary conditions along the crack line. The dimension in the y direction is longer than that in the x direction, which means it is more possible that there will be higher modes in the y direction than in x direction. Based on Levy method, the solutions for the differential equations of the plate are assumed as

$$w(x, y, t) = \sum_{n=1}^{N} Y_n(y) \cdot \sin\left(\frac{\pi x}{a}\right) \cdot e^{i\omega t}. \tag{12}$$

$Y_n(y)$ can be written as

$$Y_n(y) = A_n \cosh\left(\frac{\beta_n y}{b}\right) + B_n \sinh\left(\frac{\beta_n y}{b}\right) + C_n \sin\left(\frac{\gamma_n y}{b}\right) + D_n \cos\left(\frac{\gamma_n y}{b}\right), \tag{13}$$

where $\beta_n = (b/a)\sqrt{\lambda_n^2 + (\pi)^2}$, $\gamma_n = (b/a)\sqrt{\lambda_n^2 - (\pi)^2}$, $\lambda_n^4 = a^4\omega_n^2\rho H/D$, and A_n, B_n, C_n, and D_n are undetermined coefficients.

According to boundary conditions (6a) and (6b), we can obtain $A_n = D_n = 0$. Then, the modal functions of transversal displacement w in the y direction for plate I and plate II are obtained:

$$Y_n^{\mathrm{I}}(y) = B_n^{\mathrm{I}} \sinh\left(\frac{\beta_n y}{b}\right) + C_n^{\mathrm{I}} \sin\left(\frac{\gamma_n y}{b}\right), \quad (0 \le y \le y_0), \tag{14a}$$

$$Y_n^{\mathrm{II}}(y) = B_n^{\mathrm{II}} \sinh\left[\frac{\beta_n (y-b)}{b}\right] + C_n^{\mathrm{II}} \sin\left[\frac{\gamma_n (y-b)}{b}\right], \quad (y_0 < y \le 1). \tag{14b}$$

Substituting (14a) and (14b) into inner boundary condition equations (8a), (8d), (8e), and (8h), Homogeneous algebraic equations of the undetermined coefficients (B_n^{I}, B_n^{II}, and C_n^{II}) are derived, which results in an eigenvalue problem with the eigenvalues related to the natural frequencies of plate. Then, substituting the result of each order frequency to Homogeneous algebraic equations, the undetermined coefficients can be obtained by solving these equations and given in terms of expression relevant to C_n^{I}, respectively.

$$B_n^{\mathrm{I}} = e_n^1 C_n^{\mathrm{I}}, \tag{15a}$$

$$C_n^{\mathrm{II}} = e_n^2 C_n^{\mathrm{I}}, \tag{15b}$$

$$B_n^{\mathrm{II}} = e_n^3 B_n^{\mathrm{I}} = e_n^3 e_n^1 C_n^{\mathrm{I}}, \tag{15c}$$

where parameters e_n^1, e_n^2, and e_n^3 can be expressed as

$$\begin{aligned} e_n^1 = -\Bigg\{ & \sinh\left(\frac{\beta_n (y_0-b)}{b}\right)\Bigg[b\sin\left(\frac{\gamma_n (y_0-b)}{b}\right) \\ & \cdot a^2 EH^2 \cos\left(\frac{\gamma_n y_0}{b}\right)\gamma_n - ba^2 EH^2 \sin\left(\frac{\gamma_n y_0}{b}\right) \\ & \cdot \cos\left(\frac{\gamma_n (y_0-b)}{b}\right)\gamma_n - 72\alpha_{bb}\sin\left(\frac{\gamma_n (y_0-b)}{b}\right) \\ & \cdot D_{21} n^2\pi^2 b^2 \sin\left(\frac{\gamma_n y_0}{b}\right) - 72\alpha_{bb} \\ & \cdot \sin\left(\frac{\gamma_n (y_0-b)}{b}\right) D_{22} a^2 \sin\left(\frac{\gamma_n y_0}{b}\right)\gamma_n^2 + 72\alpha_{bb} \\ & \cdot \sin\left(\frac{\gamma_n (y_0-b)}{b}\right)\nu_{12}^2 D_{21} n^2\pi^2 b^2 \sin\left(\frac{\gamma_n y_0}{b}\right) \\ & + 72\alpha_{bb}\sin\left(\frac{\gamma_n (y_0-b)}{b}\right)\nu_{12}^2 D_{22} a^2 \sin\left(\frac{\gamma_n y_0}{b}\right) \\ & \cdot \gamma_n^2\Bigg]\Bigg\}\Bigg\{\sin\left(\frac{\gamma_n (y-b)}{b}\right)\Bigg[b\sinh\left(\frac{\beta_n (y_0-b)}{b}\right) \end{aligned}$$

Table 1: First three-order frequencies of cracked and intact plates.

	First-order natural frequency (Hz)		Second-order natural frequency (Hz)		Third-order natural frequency (Hz)	
	Theoretical results	FEM	Theoretical results	FEM	Theoretical results	FEM
Intact plate	23.9874	25.101	38.3798	41.853	62.3672	68.485
$\eta = 0.25$	23.9279	24.987	38.1120	41.359	62.1117	68.071
$\eta = 0.5$	23.8698	24.941	38.3798	41.749	61.8510	67.468

$$\cdot a^2 EH^2 \cosh\left(\frac{\beta_n y_0}{b}\right)\beta_n - ba^2 EH^2 \sinh\left(\frac{\beta_n y_0}{b}\right)$$
$$\cdot \cosh\left(\frac{\beta_n (y_0 - b)}{b}\right)\beta_n - 72\alpha_{bb}$$
$$\cdot \sinh\left(\frac{\beta_n (y_0 - b)}{b}\right) D_{21} n^2 \pi^2 b^2 \sinh\left(\frac{\beta_n y_0}{b}\right)$$
$$+ 72\alpha_{bb} \sinh\left(\frac{\beta_n (y_0 - b)}{b}\right) D_{22} a^2 \sinh\left(\frac{\beta_n y_0}{b}\right)$$
$$\cdot \beta_n^2 + 72\alpha_{bb} \sinh\left(\frac{\beta_n (y_0 - b)}{b}\right) \nu_{12}^2 D_{21} n^2 \pi^2 b^2$$
$$\cdot \sinh\left(\frac{\beta_n y_0}{b}\right) - 72\alpha_{bb} \sinh\left(\frac{\beta_n (y_0 - b)}{b}\right)$$
$$\cdot \nu_{12}^2 D_{22} a^2 \sinh\left(\frac{\beta_n y_0}{b}\right)\beta_n^2\Bigg]\Bigg\}^{-1}, \tag{16a}$$

$$e_n^2 = \frac{\sin(\gamma_n y_0/b)}{\sin[\gamma_n (y_0 - b)/b]}, \tag{16b}$$

$$e_n^3 = \frac{\sinh(\beta_n y_0/b)}{\sinh[\beta_n (y_0 - b)/b]}. \tag{16c}$$

Substituting (15a), (15b), and (15c) into (14a) and (14b), we obtained the modal function of plate I and plate II in the y direction.

$$Y_n^{\mathrm{I}}(y) = a_n^{\mathrm{I}} \sinh\left(\frac{\beta_n y}{b}\right) + \sin\left(\frac{\gamma_n y}{b}\right), \tag{17a}$$

$$Y_n^{\mathrm{II}}(y) = a_n^{\mathrm{II}} \sinh\left[\frac{\beta_n (y - b)}{b}\right] + \sin\left[\frac{\gamma_n (y - b)}{b}\right], \tag{17b}$$

where $a_n^{\mathrm{I}} = e_n^1$ and $a_n^{\mathrm{II}} = e_n^3 e_n^1 / e_n^2$.

The first three-order modes and natural frequencies of the cracked plate can be obtained by the method mentioned above, which is verified by finite element method. We chose parameters of material and size as $a = 1$ m, $b = 2$ m, $\mu = 0.33$ and $H = 0.008$ m $E = 2.1 \times 10^5$ MPa, and $\rho = 7860\,\mathrm{kg/m^3}$.

Tables 1 and 2 show the first three-order frequencies and modes for plates with cracks at different location ($\eta = y_0/b$), respectively. They show that the crack almost has no influence on natural frequencies and modes when the crack coincides with a line of node, while the crack has more effect at the maximum defection position. For example, the crack at $y_0/b = 0.5$ does not affect the second frequency and mode, because this location is the node line of second mode; however, it has more influence on the first- and the third-order frequency and mode. When the crack moves to the position ($y_0/b = 0.25$), the effects on the second mode are more evident than that on the first and third mode.

Theoretical results and simulation data are in good agreement, and the accuracy of the theoretical method is verified in this section. Comparing theoretical results to simulation data, the first three-order modal figures obtained by theoretical calculation are consistent with FEM simulations. Thus, the modal functions corresponding to the first three-order modal figures are used to construct the solutions of dynamic equations.

3. Stress Functions

The stress functions of cracked thin plate with large deflection are obtained by the equations of compatibility. Using the first three modes of mode shape function (17a) and (17b), the solutions of dynamic equations are assumed as

$$w^{\mathrm{I}}(x, y, t) = w_1(t) \cdot Y_1^{\mathrm{I}}(y) \sin\left(\frac{\pi x}{a}\right) + w_2(t)$$
$$\cdot Y_2^{\mathrm{I}}(y) \sin\left(\frac{\pi x}{a}\right) + w_3(t) \tag{18a}$$
$$\cdot Y_3^{\mathrm{I}}(y) \sin\left(\frac{\pi x}{a}\right),$$

$$w^{\mathrm{II}}(x, y, t) = w_1(t) \cdot Y_1^{\mathrm{II}}(y) \sin\left(\frac{\pi x}{a}\right) + w_2(t)$$
$$\cdot Y_2^{\mathrm{II}}(y) \sin\left(\frac{\pi x}{a}\right) + w_3(t) \tag{18b}$$
$$\cdot Y_3^{\mathrm{II}}(y) \sin\left(\frac{\pi x}{a}\right),$$

where $w_1(t)$, $w_2(t)$, and $w_3(t)$ are time-related variables. Introducing (18a) and (18b) into the compatibility equations (4), and using the boundary conditions (6a) and (6b), the stress function expression of thin plate with an all-over surface crack is gained

$$\varphi^r(x, y, t) = \sum_{i=1}^{12} \varphi_i^r, \quad (r = \mathrm{I}, \mathrm{II}), \tag{19}$$

where the parameter φ_i^r is given in Appendix.

During vibration, surface crack will be continuously open-closed. When the crack is open, the modes of crack thin plate are adopted and the stress function of crack thin

Table 2: First three-order modes frequency of cracked and intact plates.

	Theoretical results		FEM
	Mode of y direction ($\eta = 0.25$ —, $\eta = 0.5$ – · –)	Mode of x direction	
First order	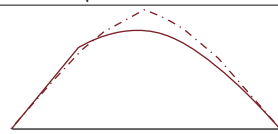	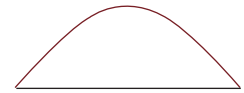	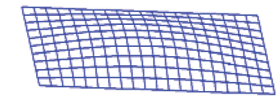
Second order	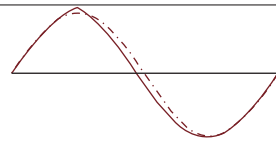	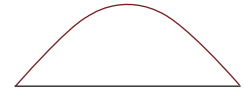	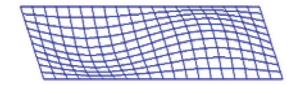
Third order	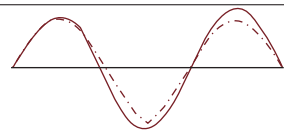		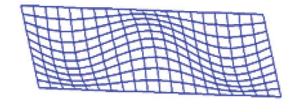

plate considering large deflection is obtained as (19). When the crack is closed, the modes of intact plate are adopted. Using the mode functions of intact plate, the authors get the stress function expression of intact plate considering large deflection. As to intact plate, the first three modes are taken and the solutions of dynamic equations are

$$w(x,y,t) = w_1(t) \cdot \sin\left(\frac{\pi x}{a}\right)\sin\left(\frac{\pi y}{b}\right) + w_2(t) \cdot \sin\left(\frac{\pi x}{a}\right)\sin\left(\frac{2\pi y}{b}\right) + w_3(t) \cdot \sin\left(\frac{\pi x}{a}\right)\sin\left(\frac{3\pi y}{b}\right). \tag{20}$$

Substituting expression (20) into the compatibility equations (4), the stress function of intact plate with large deflection is obtained

$$\begin{aligned}\varphi(x,y) = {} & \cos\left(\frac{2\pi x}{a}\right)\cdot\left[A_1\cos\left(\frac{\pi y}{b}\right)\cos\left(\frac{2\pi y}{b}\right)\right. \\ & + B_1\cos\left(\frac{\pi y}{b}\right)\cos\left(\frac{3\pi y}{b}\right) \\ & + C_1\cos\left(\frac{3\pi y}{b}\right)\cos\left(\frac{2\pi y}{b}\right) \\ & + A_2\sin\left(\frac{\pi y}{b}\right)\sin\left(\frac{2\pi y}{b}\right) \\ & + B_2\sin\left(\frac{\pi y}{b}\right)\sin\left(\frac{3\pi y}{b}\right) \\ & \left. + C_2\sin\left(\frac{3\pi y}{b}\right)\sin\left(\frac{2\pi y}{b}\right) + W_c\right] \\ & + \left[A_3\cos\left(\frac{\pi y}{b}\right)\cos\left(\frac{2\pi y}{b}\right)\right. \\ & + B_3\cos\left(\frac{\pi y}{b}\right)\cos\left(\frac{3\pi y}{b}\right) \\ & + C_3\cos\left(\frac{3\pi y}{b}\right)\cos\left(\frac{2\pi y}{b}\right) \\ & + A_4\sin\left(\frac{\pi y}{b}\right)\sin\left(\frac{2\pi y}{b}\right) \\ & + B_4\sin\left(\frac{\pi y}{b}\right)\sin\left(\frac{3\pi y}{b}\right) \\ & + C_4\sin\left(\frac{3\pi y}{b}\right)\sin\left(\frac{2\pi y}{b}\right) + A_5\cos^2\left(\frac{\pi y}{b}\right) \\ & \left. + A_6\cos^2\left(\frac{2\pi y}{b}\right) + A_7\cos^2\left(\frac{3\pi y}{b}\right)\right], \end{aligned} \tag{21}$$

where the coefficients can be found in Appendix.

4. Discrete Equation

Having obtained the mode shape functions and stress function expression of crack thin plate and intact plate, the authors use Galerkin method to discrete the dynamic equation (5). As to crack thin plate, the authors adopt the mode shape function and stress function of crack thin plate. Substituting expressions (18a) and (18b) and (19) into (5), the discrete dynamic equations of open-crack thin plate are obtained as

$$\begin{aligned}\ddot{w}_1 = {} & a_{11}w_1 + a_{12}w_2 + a_{13}w_3 + a_{14}w_1^3 + a_{15}w_2^3 \\ & + a_{16}w_3^3 + a_{17}w_1w_2^2 + a_{18}w_1w_3^2 + a_{19}w_2w_1^2 \\ & + a_{110}w_2w_3^2 + a_{111}w_3w_1^2 + a_{112}w_3w_2^2 \\ & + a_{113}w_1w_2w_3 + a_{114}P, \\ \ddot{w}_2 = {} & a_{21}w_1 + a_{22}w_2 + a_{23}w_3 + a_{24}w_1^3 + a_{25}w_2^3 \\ & + a_{26}w_3^3 + a_{27}w_1w_2^2 + a_{28}w_1w_3^2 + a_{29}w_2w_1^2 \end{aligned} \tag{22a}$$

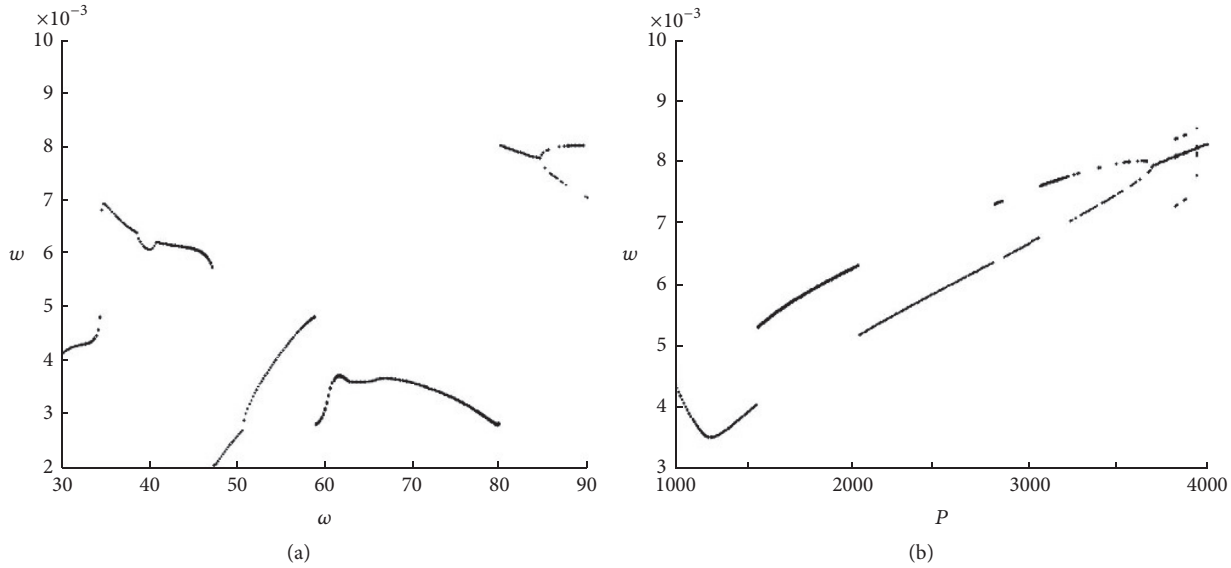

Figure 2: The bifurcation diagram of intact plate for transverse displacement w, (a) via the external excitation of changing frequency and (b) via the external excitation of changing amplitude.

$$+ a_{210}w_2w_3^2 + a_{211}w_3w_1^2 + a_{212}w_3w_2^2 + a_{213}w_1w_2w_3 + a_{214}P, \tag{22b}$$

$$\ddot{w}_3 = a_{31}w_1 + a_{32}w_2 + a_{33}w_3 + a_{34}w_1^3 + a_{35}w_2^3 + a_{36}w_3^3 + a_{37}w_1w_2^2 + a_{38}w_1w_3^2 + a_{39}w_2w_1^2 + a_{310}w_2w_3^2 + a_{311}w_3w_1^2 + a_{312}w_3w_2^2 + a_{313}w_1w_2w_3 + a_{314}P, \tag{22c}$$

where a with subscript are coefficients determined by material, geometry, and crack parameters of the plate.

As to intact plate, the modal function and stress function of intact plate are adopted. Putting expressions (20) and (21) into (5), the discrete dynamic equations of intact plate are gained:

$$\ddot{w}_1 = b_{11}w_1 + b_{12}w_1^3 + b_{13}w_1w_2^2 + b_{14}w_1w_3^2 + b_{15}w_1^2w_3 + b_{16}w_2^2w_3 + b_{17}P, \tag{23a}$$

$$\ddot{w}_2 = b_{21}w_2 + b_{22}w_2^3 + b_{23}w_1^2w_2 + b_{24}w_2w_3^2 + b_{25}w_1w_2w_3, \tag{23b}$$

$$\ddot{w}_3 = b_{31}w_3 + b_{32}w_3^3 + b_{33}w_1w_2^2 + b_{34}w_3w_1^2 + b_{35}w_2^2w_3 + b_{36}w_2^2w_1 + b_{37}w_1^3 + b_{38}P, \tag{23c}$$

where b with subscript are coefficients in relation to material and geometry of the plate.

The opening and closing of breathing crack are described as piecewise model during the vibration. The authors assume that the crack is on the top surface of the plate and the transversal displacement w is positive when w is below origin of coordinates. During vibration, the dynamic equations are discrete dynamic equations which are (22a)–(22c), when $w \leq 0$ (crack is open); the dynamic equations are (23a)–(23c), when $w > 0$ (crack is closed).

5. Effect of Crack Parameters on Nonlinear Dynamic Behaviors

The Runge-Kutta algorithm is utilized to numerically analyze the nonlinear dynamical behaviors of the cracked plate under different excitation amplitude and frequency. The nonlinear dynamical behaviors of the plate with different crack location and depth are studied by analyzing the bifurcation diagrams. To compare with the effect of breathing crack on the plate, the nonlinear dynamic responses of the plate with an open crack and the intact plate are analyzed too. In numerical simulation, we chose parameters of material and size as $\rho = 7860\,\text{kg/m}^3$, $E = 2.1 \times 10^5\,\text{MPa}$, $a = 1\,\text{m}$, $b = 2\,\text{m}$, $\mu = 0.33$, and $H = 0.008\,\text{m}$.

For intact plate, as shown in Figure 2(a), the excitation frequencies change from 30 rad/s to 90 rad/s, when the external excitation amplitude is $P = 3000\,\text{N/m}^2$. The excitation amplitude changes from $1000\,\text{N/m}^2$ to $4000\,\text{N/m}^2$, while the excitation frequency is $\omega = 80\,\text{rad/s}$, such as Figure 2(b). Figures 2(a) and 2(b) represent the bifurcation diagram of intact plate via the different excitation frequencies and amplitudes on transversal displacement w, respectively. The coordinate and the variation of external excitation for the following bifurcation figures are the same as those in Figure 2.

5.1. Effect of Crack Depth on Nonlinear Dynamic Behavior. The nonlinear dynamic behaviors of cracked plate are studied to analyze the effect of external excitation amplitudes and frequencies on plate with different crack depth. The rectangular

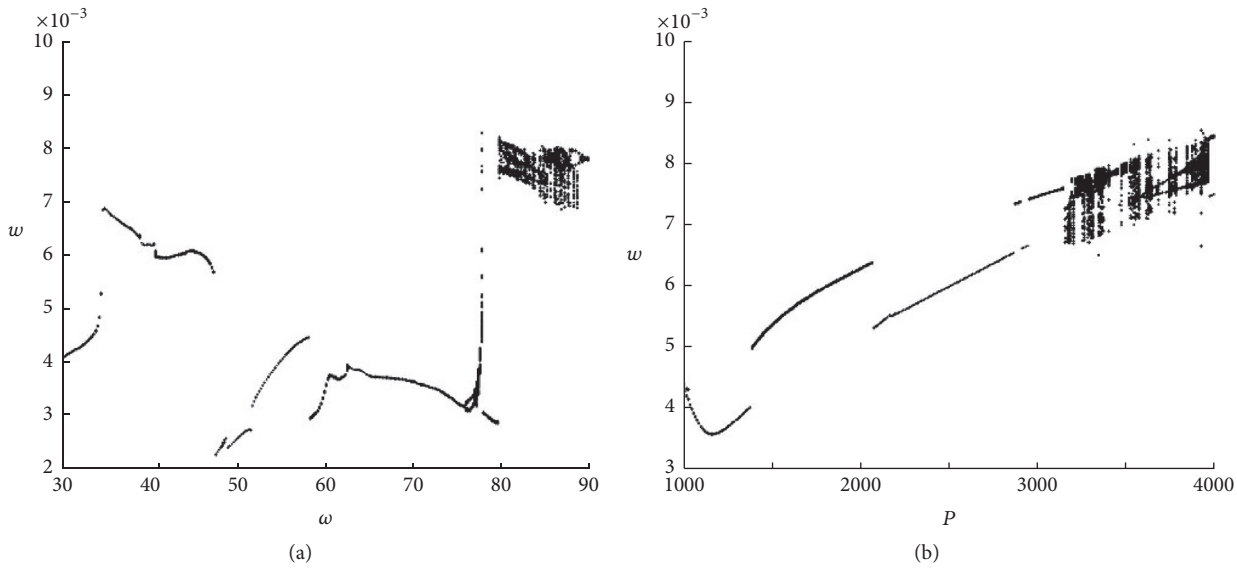

Figure 3: The bifurcation diagram of plate with a breathing crack ($h_0/H = 0.2$) for transverse displacement w, (a) via the external excitation of changing frequency and (b) via the external excitation of changing amplitude.

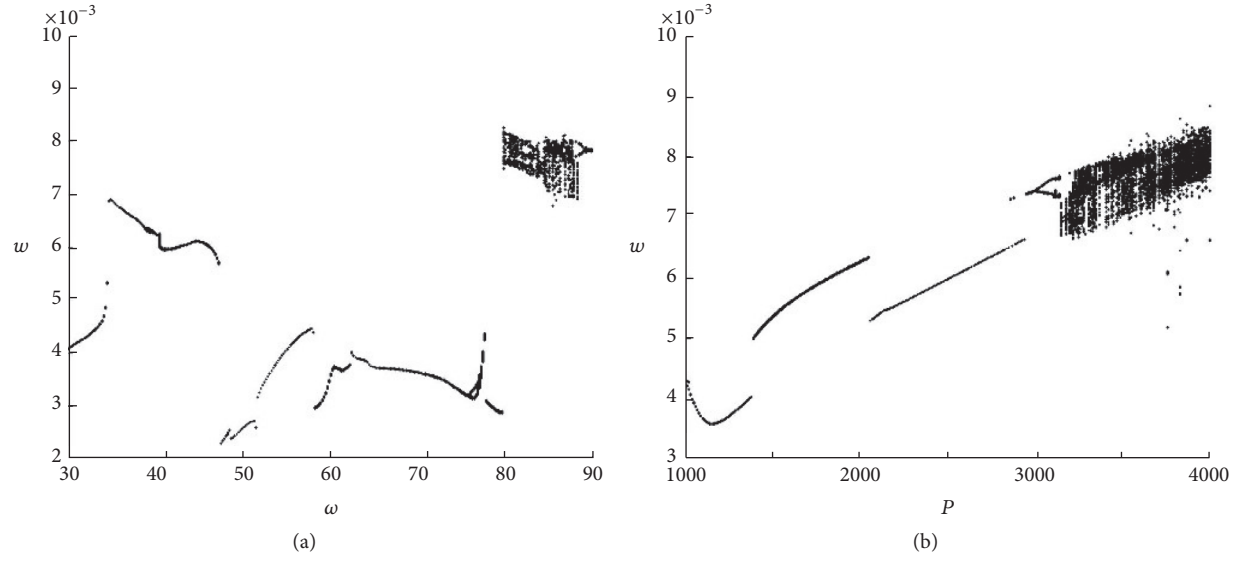

Figure 4: The bifurcation diagram of plate with a breathing crack ($h_0/H = 0.4$) for transverse displacement w, (a) via the external excitation of changing frequency and (b) via the external excitation of changing amplitude.

plates have a crack at $\eta_0 = 0.5$, where $\eta_0 = y_0/b$. We chose the crack depths as $h_0/H = 0.2, 0.4$, and 0.6, respectively.

Figures 3, 4, and 5 are the bifurcation diagrams for plates with breathing cracks at different crack depth. Figures 6, 7, and 8 demonstrate bifurcation diagrams for open-crack plates at various crack depth.

The above bifurcation diagrams show that breathing crack plate has complex nonlinear phenomenon: quasi-periodic motion, bifurcation motion, and chaotic motion. With the change of crack depth, the bifurcation diagrams of breathing crack plates represent different nonlinear dynamic behaviors. However, the motion of open-crack plates is relatively simple, which merely demonstrates the single-cycle movement and the movement of doubling the cycle.

As for bifurcation diagram 4, the corresponding waveform and phase diagrams are gained when the external excitation amplitudes are 2500, 3100, 3300, 3400, 3700, and 3800 N/m^2, respectively, as shown in Figure 9. Figures 9(a)–9(d) show the periodic motion of cycle 1, 2, 5, and 7 times the cycle of movement, while Figures 9(e) and 9(f) represent the quasi-periodic and chaotic motions.

For one cycle motion, as shown in Figure 9(a), the authors find that the transversal displacement amplitudes in positive and negative directions are, respectively, 4.3 mm and 5 mm.

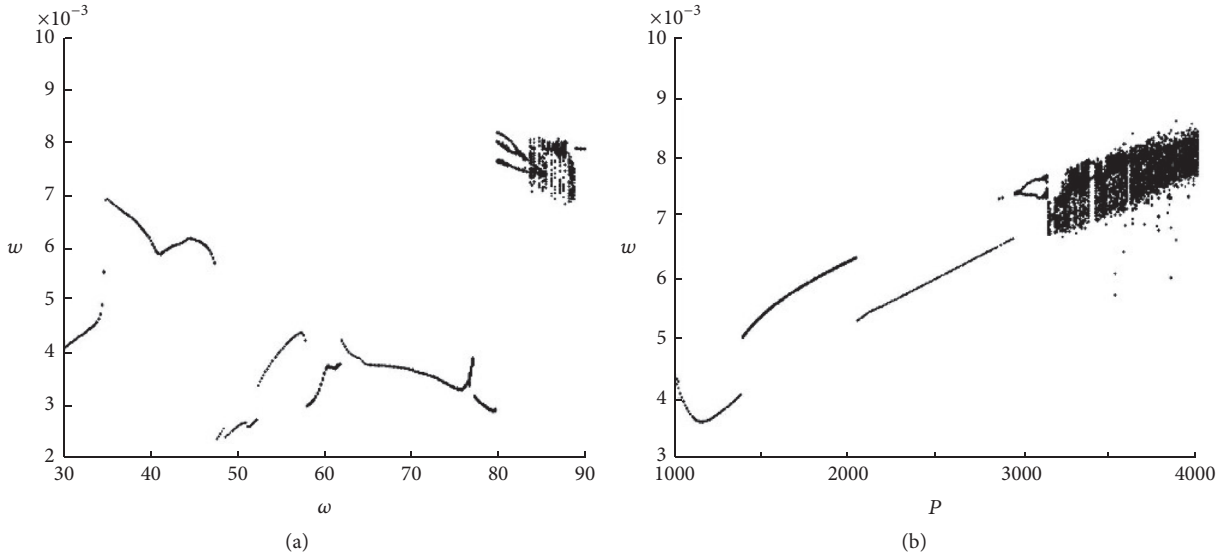

Figure 5: The bifurcation diagram of plate with a breathing crack ($h_0/H = 0.6$) for transverse displacement w, (a) via the external excitation of changing frequency and (b) via the external excitation of changing amplitude.

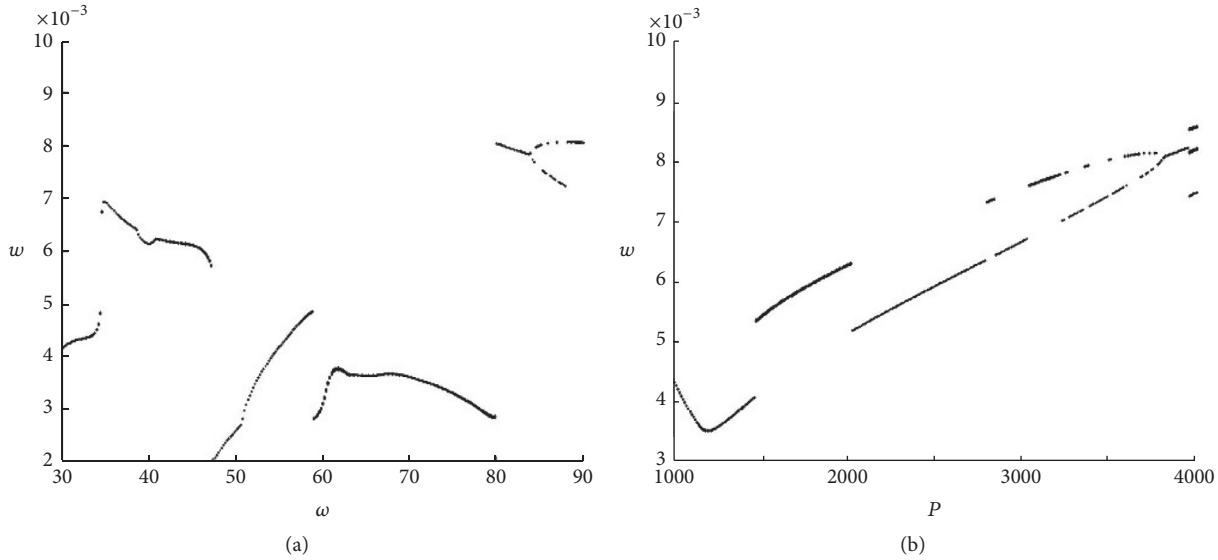

Figure 6: The bifurcation diagram of plate with an open crack ($h_0/H = 0.2$) for transverse displacement w, (a) via the external excitation of changing frequency and (b) via the external excitation of changing amplitude.

It represents that when $w > 0$, the crack is closed and the stiffness of plate is relatively large, so the amplitude is 4.3 mm; when $w \leq 0$, the crack is open and the stiffness decreases, so the amplitude increases to 5 mm.

5.2. Effect of Crack Location on Nonlinear Dynamic Behaviors. In this section, the effect of crack location on nonlinear dynamic behavior is studied to analyze the bifurcation diagrams of plates subject to external excitation. The simply supported rectangular plates have a crack at depth ($h_0/H = 0.65$) and various locations ($\eta_0 = 0.15, 0.30$, and 0.45).

Figures 10, 11, and 12 are the bifurcation diagrams of plates with breathing cracks at different crack location. Figures 13, 14, and 15 demonstrate bifurcation diagrams for open-crack plates at various crack locations.

6. Conclusions

The piecewise model is used to describe the opening and closing of crack during the vibration. The dynamic equations are solved by using the stress function and the mode functions derived by this paper. Bifurcation diagrams, wave-shape

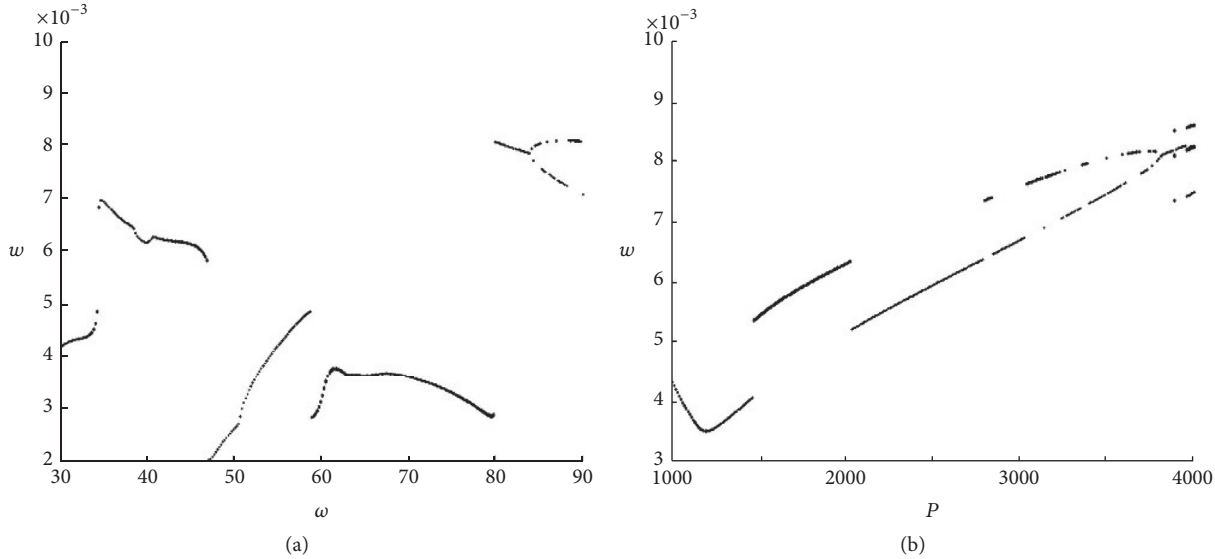

Figure 7: The bifurcation diagram of plate with an open crack ($h_0/H = 0.4$) for transverse displacement w, (a) via the external excitation of changing frequency and (b) via the external excitation of changing amplitude.

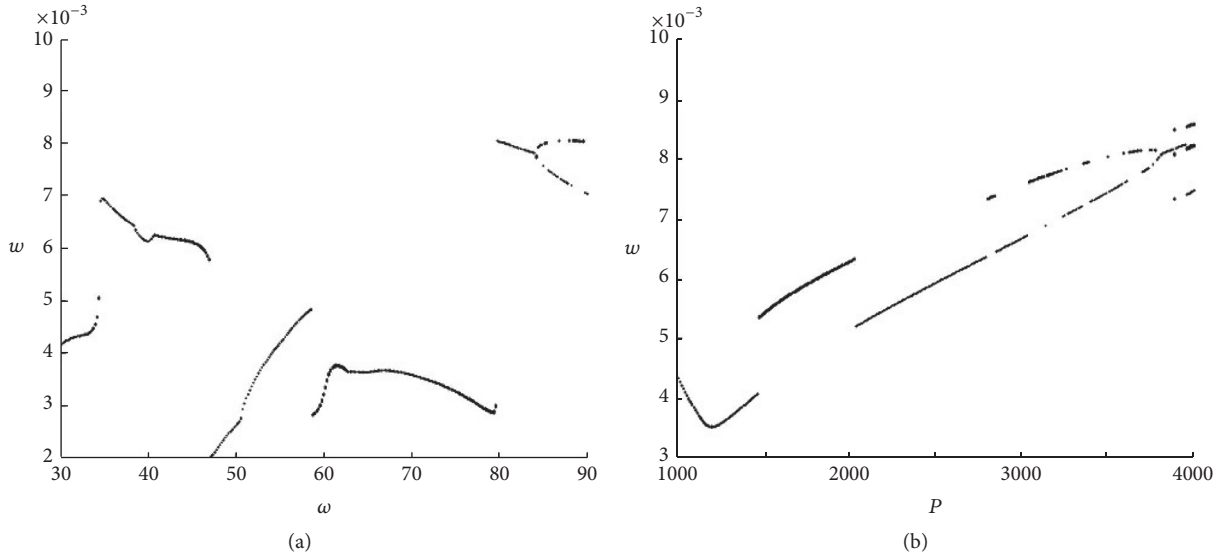

Figure 8: The bifurcation diagram of plate with an open crack ($h_0/H = 0.6$) for transverse displacement w, (a) via the external excitation of changing frequency and (b) via the external excitation of changing amplitude.

diagrams, and phase diagrams of simply supported rectangular thin plate with an all-over breathing crack are investigated in this paper. The following conclusions have been obtained:

(1) It is complex to derive the mode functions of in-plane displacements (u_0, v_0) for large deflection cracked plate. This paper introduces the stress functions obtained by compatibility equation of cracked plate to eliminate the in-plane displacement (u_0, v_0), which provide a new solution for the problem of large deflection vibration in cracked plates.

(2) The previous study of the nonlinear dynamics of surface crack plate usually uses open-crack model. However, the authors find that the nonlinear dynamic behaviors of open-crack model are similar to those of the intact plate, which does not reveal the effect of crack on nonlinear dynamic behaviors of plate. Breathing crack model reflects the real process of opening-closing of surface plate and presents more complex phenomena. Through three sets of bifurcation diagrams, we find that breathing crack plate has complex nonlinear phenomena such as

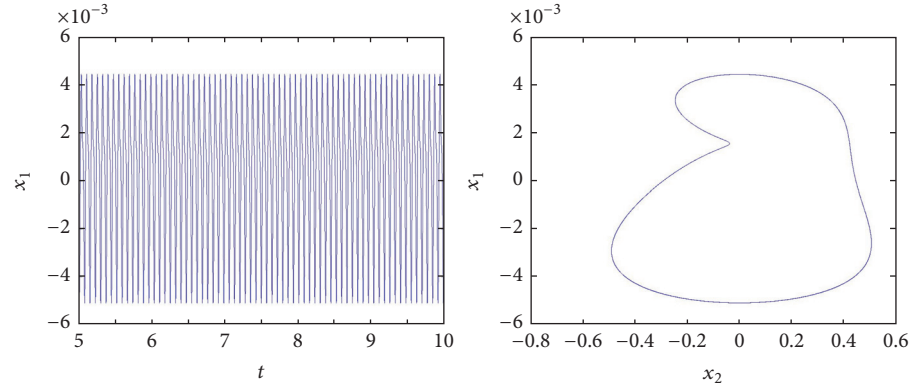

(a) $\omega = 70$ rad/s, $P = 2500$ N/m^2

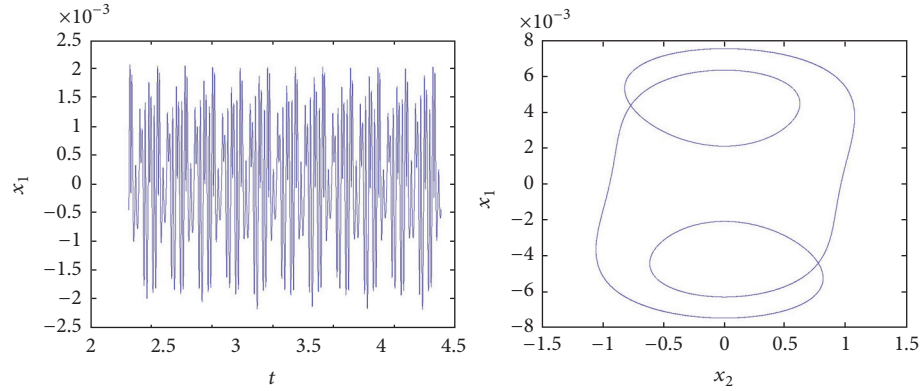

(b) $\omega = 70$ rad/s, $P = 3100$ N/m^2

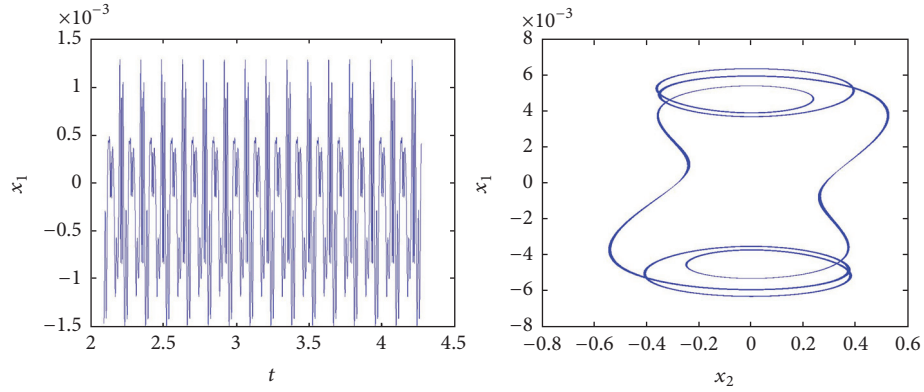

(c) $\omega = 70$ rad/s, $P = 3300$ N/m^2

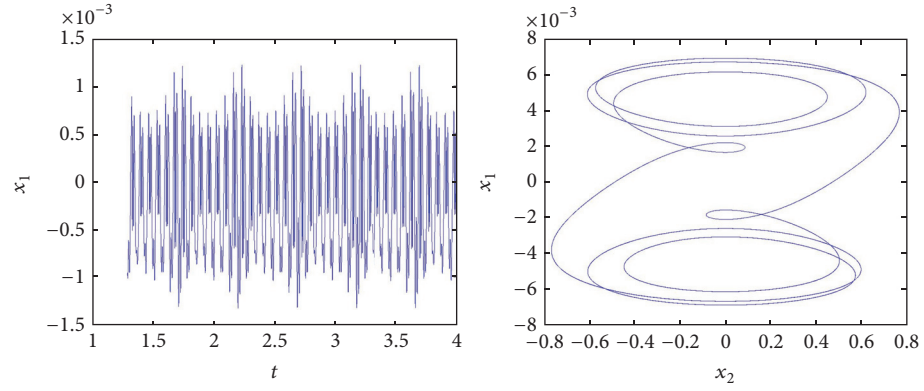

(d) $\omega = 70$ rad/s, $P = 3400$ N/m^2

Figure 9: Continued.

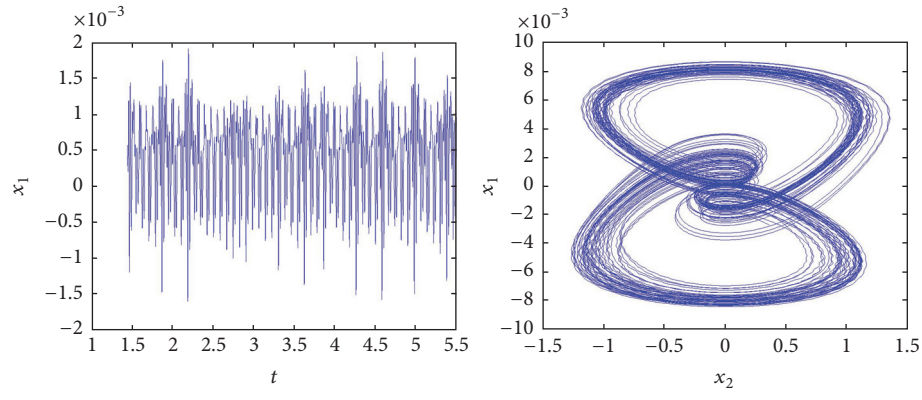

(e) $\omega = 70$ rad/s, $P = 3700$ N/m^2

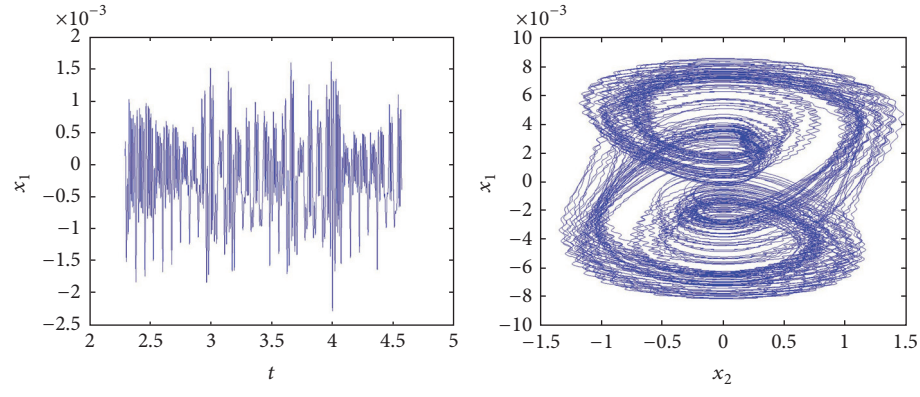

(f) $\omega = 70$ rad/s, $P = 3800$ N/m^2

FIGURE 9: Waveforms and bifurcation of the plate with breathing crack; relative crack depth $h_0/H = 0.6$; crack location $\eta_0 = 0.5$.

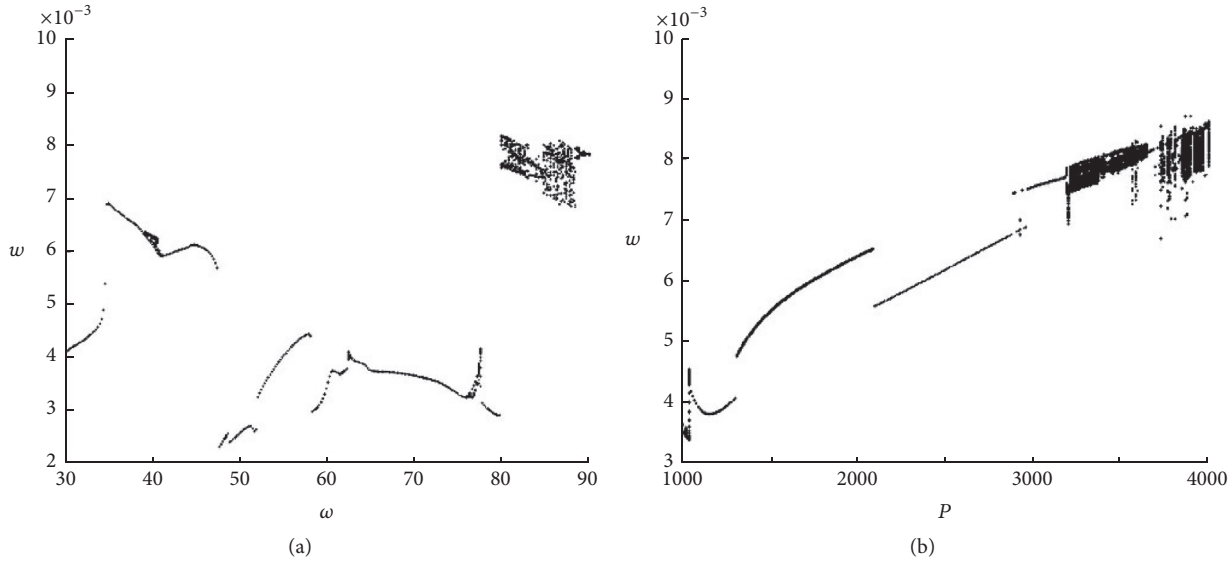

(a) (b)

FIGURE 10: The bifurcation diagram of plate with a breathing crack ($\eta_0 = 0.15$) for transverse displacement w, (a) via the external excitation of changing frequency and (b) via the external excitation of changing amplitude.

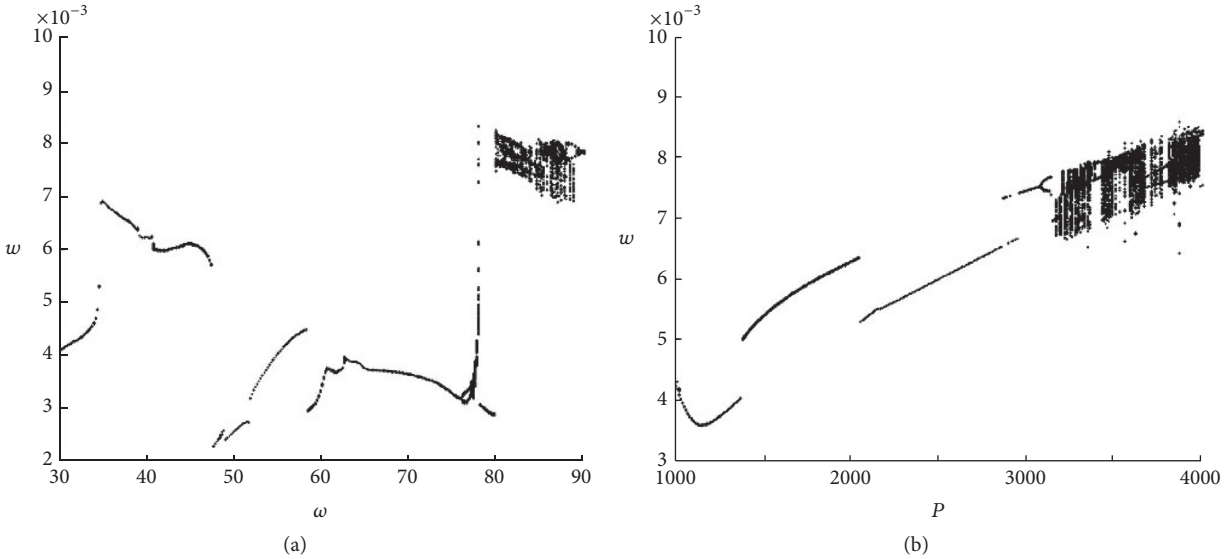

Figure 11: The bifurcation diagram of plate with a breathing crack ($\eta_0 = 0.30$) for transverse displacement w, (a) via the external excitation of changing frequency and (b) via the external excitation of changing amplitude.

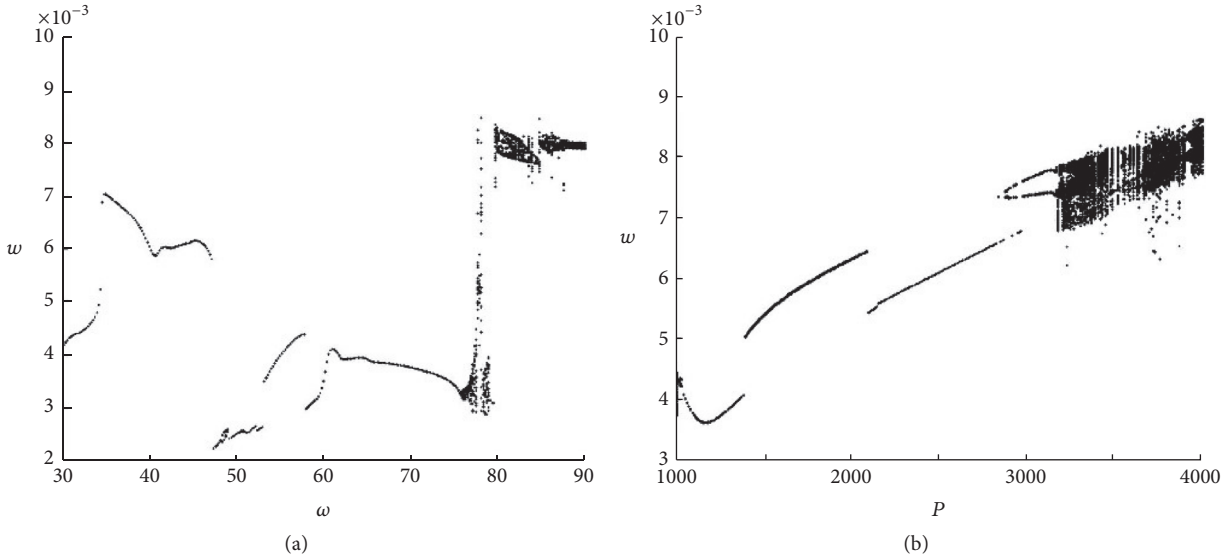

Figure 12: The bifurcation diagram of plate with a breathing crack ($\eta_0 = 0.45$) for transverse displacement w, (a) via the external excitation of changing frequency and (b) via the external excitation of changing amplitude.

quasi-periodic motion, bifurcation motion, and chaotic motion, and the nonlinear dynamic behaviors of open-crack model are similar to intact plate model, which merely presents the single-cycle motion and the double periodic motion.

(3) The deeper the crack is, the smaller the critical excitation frequency will be, which means that the increase of the crack depth will make the motion of crack plate more complicated. There are two reasons for this phenomenon. Firstly, the increase of the crack depth reduces the stiffness of plate, resulting in the increase of vibration amplitude for the cracked plate which leads to complex nonlinear dynamic behavior. Secondly, the crack alternately opens and closes during vibrational cycle and the increase of the crack depth forms the cracked structure with strong nonsmooth characteristics.

(4) When the crack is near the center of the plate, complex nonlinear dynamic behavior more easily occurs in the vibration of cracked plate subject to certain excitation amplitude and frequency. This is because the maximum transversal displacement is near the center of the plate, and the farther away the crack is from the locations of zero displacement

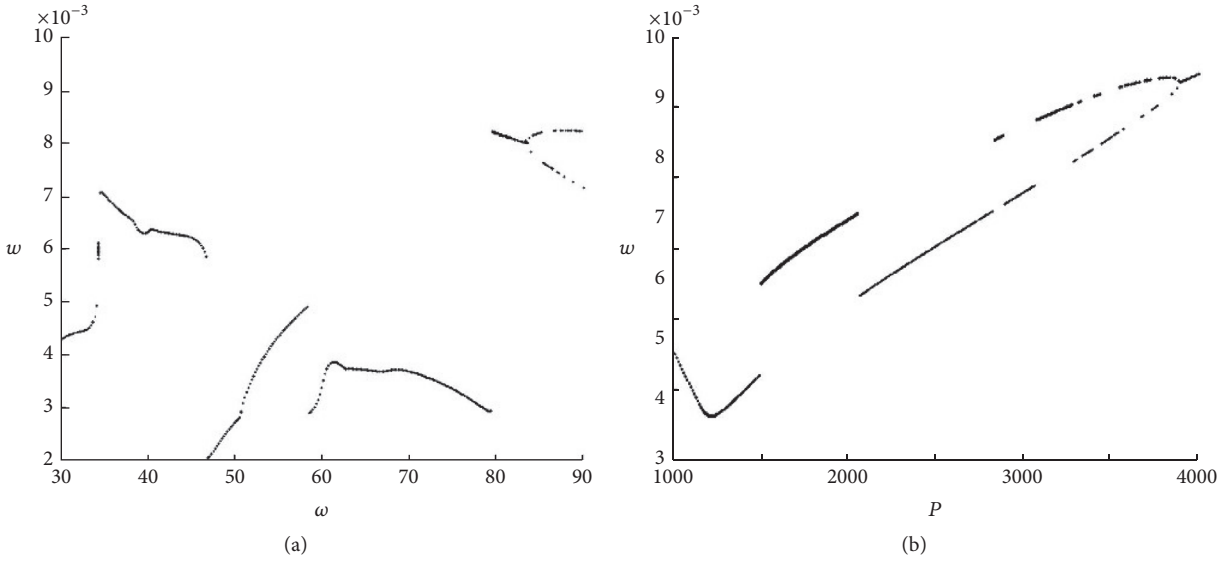

Figure 13: The bifurcation diagram of plate with an open crack ($\eta_0 = 0.15$) for transverse displacement w, (a) via the external excitation of changing frequency and (b) via the external excitation of changing amplitude.

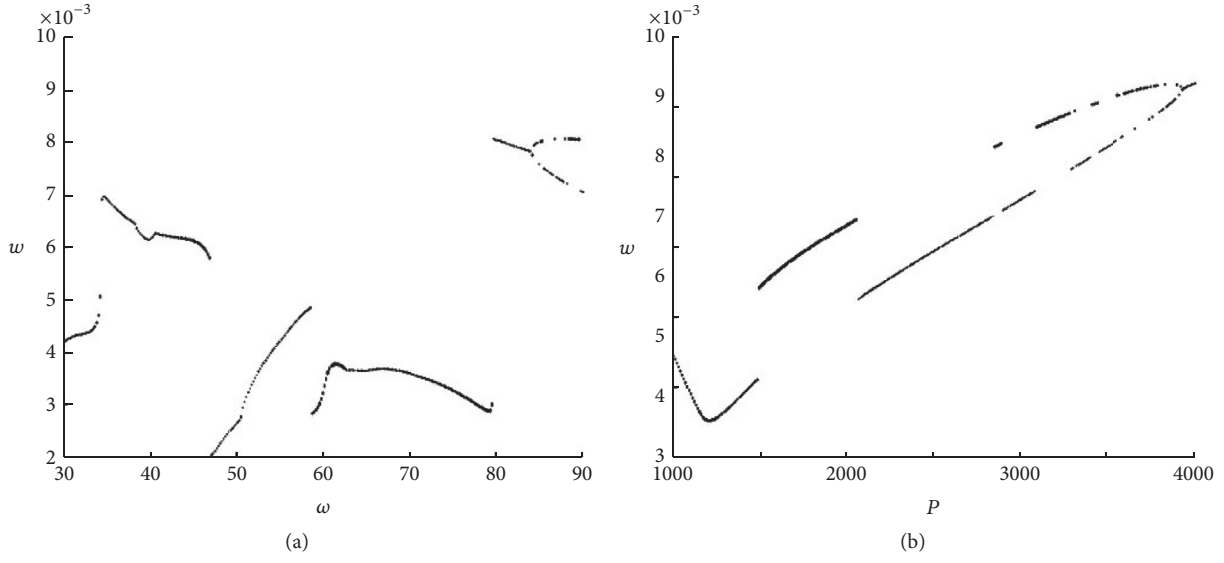

Figure 14: The bifurcation diagram of plate with an a open crack ($\eta_0 = 0.30$) for transverse displacement w, (a) via the external excitation of changing frequency and (b) via the external excitation of changing amplitude.

($w = 0$) which conclude nodal line and boundary, the greater the influence of the stiffness is.

Appendix

The coefficients given in (16a), (16b), and (16c) can be written as

$$\varphi_1^r = \sum_{i=1}^{3}\sum_{j=1}^{3} a_{ij}^{(1)} \sin\left(\frac{\gamma_i y}{b}\right)\sin\left(\frac{\gamma_j y}{b}\right) - \sum_{i=1}^{3} a_{ij}^{(1)} \cdot \sin\left(\frac{\gamma_i y}{b}\right)\sin\left(\frac{\gamma_i y}{b}\right),$$

$$\varphi_2^r = \sum_{i=1}^{3}\sum_{j=1}^{3} a_{ij}^{(2)} \cos\left(\frac{\gamma_i y}{b}\right)\cos\left(\frac{\gamma_j y}{b}\right) - \sum_{i=1}^{3} a_{ij}^{(2)} \cdot \cos\left(\frac{\gamma_i y}{b}\right)\cos\left(\frac{\gamma_i y}{b}\right),$$

$$\varphi_3^r = \left[\sum_{i=1}^{3}\sum_{j=1}^{3} a_{ij}^{(3)} \cos\left(\frac{\gamma_i y}{b}\right)\cos\left(\frac{\gamma_j y}{b}\right) - \sum_{i=1}^{3} a_{ij}^{(3)} \cos\left(\frac{\gamma_i y}{b}\right)\cos\left(\frac{\gamma_i y}{b}\right)\right]\cos\left(\frac{2\pi x}{a}\right),$$

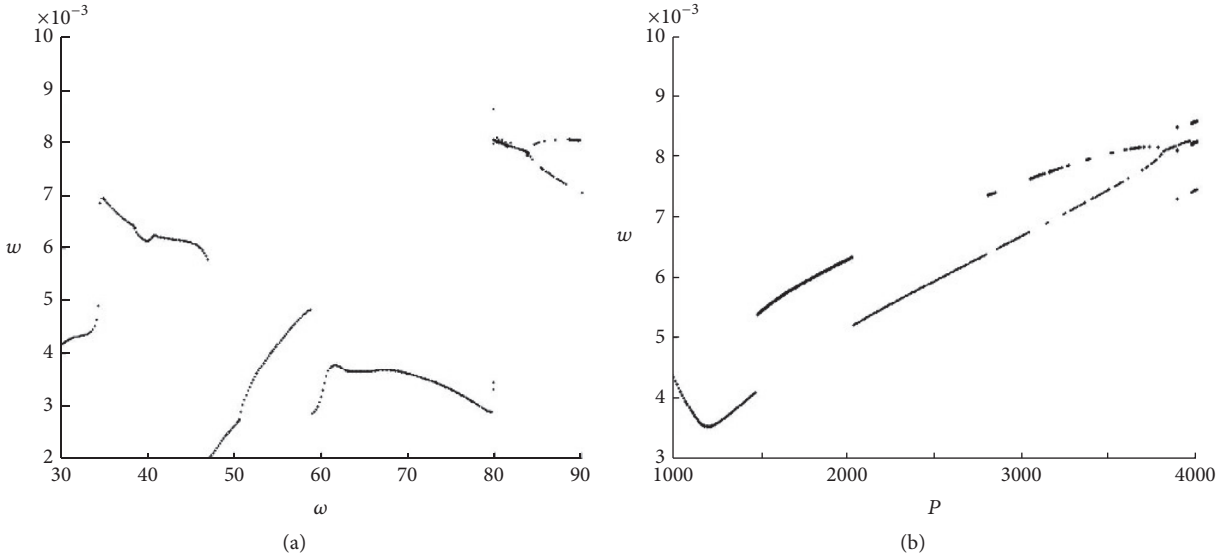

FIGURE 15: The bifurcation diagram of plate with an open crack ($\eta_0 = 0.45$) for transverse displacement w, (a) via the external excitation of changing frequency and (b) via the external excitation of changing amplitude.

$$\varphi_4^r = \left[\sum_{i=1}^{3}\sum_{j=1}^{3} a_{ij}^{(4)} \sin\left(\frac{\gamma_i y}{b}\right)\sin\left(\frac{\gamma_j y}{b}\right) - \sum_{i=1}^{3} a_{ij}^{(4)} \sin\left(\frac{\gamma_i y}{b}\right)\sin\left(\frac{\gamma_i y}{b}\right)\right]\cos\left(\frac{2\pi x}{a}\right),$$

$$\varphi_5^r = \sum_{i=1}^{3}\sum_{j=1}^{3} a_{ij}^{(5)} \sin\left(\frac{\gamma_i y}{b}\right)\sinh\left(\frac{\beta_j y}{b}\right) - \sum_{i=1}^{3}\sum_{j=1}^{3} b_{ij}^{(5)} \sinh\left(\frac{\beta_i y}{b}\right)\sin\left(\frac{\gamma_j y}{b}\right) - \sum_{i=1}^{3} a_{ii}^{(5)} \cdot \sin\left(\frac{\gamma_i y}{b}\right)\sinh\left(\frac{\beta_i y}{b}\right) + \sum_{i=1}^{3} b_{ii}^{(5)} \sinh\left(\frac{\beta_i y}{b}\right) \cdot \sin\left(\frac{\gamma_i y}{b}\right),$$

$$\varphi_6^r = \sum_{i=1}^{3}\sum_{j=1}^{3} a_{ij}^{(6)} \cos\left(\frac{\gamma_i y}{b}\right)\cosh\left(\frac{\beta_j y}{b}\right) - \sum_{i=1}^{3}\sum_{j=1}^{3} c_{ij}^{(6)} \cosh\left(\frac{\beta_i y}{b}\right)\cos\left(\frac{\gamma_j y}{b}\right) - \sum_{i=1}^{3} a_{ii}^{(6)} \cdot \cos\left(\frac{\gamma_i y}{b}\right)\cosh\left(\frac{\beta_i y}{b}\right) + \sum_{i=1}^{3} c_{ii}^{(6)} \cosh\left(\frac{\beta_i y}{b}\right) \cdot \cos\left(\frac{\gamma_i y}{b}\right),$$

$$\varphi_7^r = \left[\sum_{i=1}^{3}\sum_{j=1}^{3} a_{ij}^{(7)} \sin\left(\frac{\gamma_i y}{b}\right)\sinh\left(\frac{\beta_j y}{b}\right) - \sum_{i=1}^{3}\sum_{j=1}^{3} d_{ij}^{(7)} \sinh\left(\frac{\beta_i y}{b}\right)\sin\left(\frac{\gamma_j y}{b}\right) - \sum_{i=1}^{3} a_{ii}^{(7)} \sin\left(\frac{\gamma_i y}{b}\right)\sinh\left(\frac{\beta_i y}{b}\right) + \sum_{i=1}^{3} d_{ii}^{(7)} \sinh\left(\frac{\beta_i y}{b}\right)\sin\left(\frac{\gamma_i y}{b}\right)\right]\cos\left(\frac{2\pi x}{a}\right),$$

$$\varphi_8^r = \left[\sum_{i=1}^{3}\sum_{j=1}^{3} a_{ij}^{(8)} \cos\left(\frac{\gamma_i y}{b}\right)\cosh\left(\frac{\beta_j y}{b}\right) + \sum_{i=1}^{3}\sum_{j=1}^{3} e_{ij}^{(8)} \cosh\left(\frac{\beta_i y}{b}\right)\cos\left(\frac{\gamma_j y}{b}\right) - \sum_{i=1}^{3} a_{ii}^{(8)} \cos\left(\frac{\gamma_i y}{b}\right)\cosh\left(\frac{\beta_i y}{b}\right) - \sum_{i=1}^{3} e_{ii}^{(8)} \cosh\left(\frac{\beta_i y}{b}\right)\cos\left(\frac{\gamma_i y}{b}\right)\right]\cos\left(\frac{2\pi x}{a}\right),$$

$$\varphi_9^r = \sum_{i=1}^{3}\sum_{j=1}^{3} a_{ij}^{(9)} \sinh\left(\frac{\beta_i y}{b}\right)\sinh\left(\frac{\beta_j y}{b}\right) - \sum_{i=1}^{3} a_{ii}^{(9)} \cdot \sinh\left(\frac{\beta_i y}{b}\right)\sinh\left(\frac{\beta_i y}{b}\right),$$

$$\varphi_{10}^r = \sum_{i=1}^{3}\sum_{j=1}^{3} a_{ij}^{(10)} \cosh\left(\frac{\beta_i y}{b}\right)\sinh\left(\frac{\beta_j y}{b}\right) - \sum_{i=1}^{3} a_{ii}^{(10)} \cdot \cosh\left(\frac{\beta_i y}{b}\right)\sinh\left(\frac{\beta_i y}{b}\right),$$

$$\varphi_{11}^{r} = \left[\sum_{i=1}^{3}\sum_{j=1}^{3} a_{ij}^{(11)} \sinh\left(\frac{\beta_i y}{b}\right)\sinh\left(\frac{\beta_j y}{b}\right) - \sum_{i=1}^{3} a_{ii}^{(11)} \sinh\left(\frac{\beta_i y}{b}\right)\sinh\left(\frac{\beta_i y}{b}\right)\right]\cos\left(\frac{2\pi x}{a}\right),$$

$$\varphi_{12}^{r} = \left[\sum_{i=1}^{3}\sum_{j=1}^{3} a_{ij}^{(12)} \cosh\left(\frac{\beta_i y}{b}\right)\cosh\left(\frac{\beta_j y}{b}\right) - \sum_{i=1}^{3} a_{ii}^{(12)} \cosh\left(\frac{\beta_i y}{b}\right)\cosh\left(\frac{\beta_i y}{b}\right)\right]\cos\left(\frac{2\pi x}{a}\right),$$

$$\begin{aligned}\varphi_{13}^{r} = \sum_{i=1}^{3}\Bigg(& a^{(13)}\cos\left(\frac{2\pi x}{a}\right)\cos\left(\frac{\gamma_i y}{b}\right)\cosh\left(\frac{\beta_i y}{b}\right) \\ &+ b^{(13)}\cos\left(\frac{2\pi x}{a}\right)\sin\left(\frac{\gamma_i y}{b}\right)\sinh\left(\frac{\beta_i y}{b}\right) \\ &+ c^{(13)}\cos\left(\frac{\gamma_i y}{b}\right)\cosh\left(\frac{\beta_i y}{b}\right) \\ &+ d^{(13)}\sin\left(\frac{\gamma_i y}{b}\right)\sinh\left(\frac{\beta_i y}{b}\right) + e^{(13)}\cos\left(\frac{2\pi x}{a}\right) \\ &+ f^{(13)}\cos\left(\frac{2\gamma_i y}{b}\right) + g^{(13)}\cosh\left(\frac{2\beta_i y}{b}\right)\Bigg),\end{aligned} \tag{A.1}$$

where

$$a_{ij}^{(1)} = -\frac{1}{2}\frac{w_i\gamma_i^2 w_j b^4\left(3\gamma_j^2+\gamma_i^2\right)}{-3\gamma_i^4\gamma_j^2+3\gamma_i^2\gamma_j^4-\gamma_j^6},$$

$$a_{ij}^{(2)} = -\frac{1}{2}\frac{\left(3\gamma_i^2+\gamma_j^2\right)\gamma_i\gamma_j w_i w_j b^4}{-3\gamma_i^4\gamma_j^2+3\gamma_i^2\gamma_j^4-\gamma_j^6},$$

$$\begin{aligned}a_{ij}^{(3)} = {}& \frac{1}{2}b^4 a_j^r w_j w_i a^4\gamma_i\gamma_j\left(16\pi^4b^4+24\gamma_i^2\pi^2b^2a^2\right. \\ &+ 8\pi^2a^2b^2\gamma_j^2+5\gamma_i^4a^4+10\gamma_i^2\gamma_j^2a^4+\gamma_j^4a^4\left.\right) \\ &\cdot\left(256\pi^6b^6\gamma_i^2a^2+256\pi^6b^6\gamma_j^2a^2+96\pi^4b^4\gamma_i^4a^4\right. \\ &+ 96\pi^4b^4\gamma_j^4a^4+16\gamma_i^6\pi^2b^2a^6+16\gamma_j^6\pi^2b^2a^6 \\ &+ \gamma_j^8a^8+\gamma_i^8a^8+64\pi^4b^4\gamma_i^2\gamma_j^2a^4-16\gamma_i^4\pi^2b^2a^6\gamma_j^2 \\ &- 16\gamma_i^2\pi^2b^2a^6\gamma_j^4+256\pi^8b^8-4\gamma_i^6a^8\gamma_j^2+6\gamma_i^4a^8\gamma_j^4 \\ &\left.- 4\gamma_i^2\gamma_j^6a^8\right)^{-1},\end{aligned}$$

$$\begin{aligned}a_{ij}^{(4)} = {}& \frac{1}{2}b^4 a_j^r w_j w_i a^4\gamma_i^2\left(16\pi^4b^4+24\gamma_j^2\pi^2b^2a^2\right. \\ &+ 8\pi^2a^2b^2\gamma_i^2+5\gamma_j^4a^4+10\gamma_i^2\gamma_j^2a^4+\gamma_i^4a^4\left.\right) \\ &\cdot\left(256\pi^6b^6\gamma_i^2a^2+256\pi^6b^6\gamma_j^2a^2+96\pi^4b^4\gamma_i^4a^4\right. \\ &+ 96\pi^4b^4\gamma_j^4a^4+16\gamma_i^6\pi^2b^2a^6+16\gamma_j^6\pi^2b^2a^6 \\ &+ \gamma_j^8a^8+\gamma_i^8a^8+64\pi^4b^4\gamma_i^2\gamma_j^2a^4-16\gamma_i^4\pi^2b^2a^6\gamma_j^2 \\ &- 16\gamma_i^2\pi^2b^2a^6\gamma_j^4+256\pi^8b^8-4\gamma_i^6a^8\gamma_j^2+6\gamma_i^4a^8\gamma_j^4 \\ &\left.- 4\gamma_i^2\gamma_j^6a^8\right)^{-1},\end{aligned}$$

$$a_{ij}^{(5)} = \frac{1}{2}\frac{\left(3\beta_j^2-\gamma_i^2\right)\gamma_i^2 w_i w_j a_j^r b^4}{3\gamma_i^2\beta_j^4+3\beta_j^2\gamma_j^4+\beta_j^6+\gamma_i^6},$$

$$b_{ij}^{(5)} = -\frac{1}{2}\frac{w_i w_j a_i^r b^4\beta_i^2\left(-3\gamma_j^2+\beta_j^2\right)}{3\beta_i^4\gamma_j^2+3\beta_i^2\gamma_j^4+\beta_i^6+\gamma_j^6},$$

$$a_{ij}^{(6)} = \frac{1}{2}\frac{w_i\gamma_i w_j a_j^r b^4\left(-3\gamma_i^2+\beta_j^2\right)}{3\gamma_i^2\beta_j^4+3\beta_j^2\gamma_j^4+\beta_j^6+\gamma_i^6},$$

$$c_{ij}^{(6)} = -\frac{1}{2}\frac{w_i w_j a_i^r b^4\gamma_j\beta_i\left(3\beta_i^2-\gamma_j^2\right)}{3\beta_i^4\gamma_j^2+3\beta_i^2\gamma_j^4+\beta_i^6+\gamma_j^6},$$

$$\begin{aligned}a_{ij}^{(7)} = {}& \frac{1}{2}b^4 a_j^r w_j w_i a^4\gamma_i^2\left(16\pi^4b^4-24\beta_j^2\pi^2b^2a^2\right. \\ &+ 8\pi^2a^2b^2\gamma_i^2+5\beta_j^4a^4-10\gamma_i^2\beta_j^2a^4+\gamma_i^4a^4\left.\right) \\ &\cdot\left(-64\pi^4\gamma_i^2\beta_j^2a^4b^4+16\pi^2\gamma_i^4\beta_j^2a^6b^2\right. \\ &- 16\pi^2\gamma_i^2\beta_j^4a^6b^2+4\gamma_i^6\beta_j^2a^8+6\gamma_i^4\beta_j^4a^8+4\gamma_i^2\beta_j^6a^8 \\ &+ \beta_j^8a^8+\gamma_i^8a^8+256\pi^6b^6\gamma_i^2a^2-256\pi^6b^6a^2\beta_j^2 \\ &+ 96\pi^4b^4\gamma_i^4a^4+96\pi^4b^4\beta_j^4a^4+16\gamma_i^6\pi^2b^2a^6 \\ &\left.- 16\pi^2a^6b^2\beta_j^6+256\pi^8b^8\right)^{-1},\end{aligned}$$

$$\begin{aligned}d_{ij}^{(7)} = {}& \frac{1}{2}b^4 w_j a_i^r w_i a^4\beta_i^2\left(16\pi^4b^4+24\pi^2a^2b^2\gamma_j^2\right. \\ &- 8\beta_i^2\pi^2b^2a^2+5\gamma_j^4a^4-10\beta_i^2\gamma_j^2a^4+\gamma_j^4a^4\left.\right) \\ &\cdot\left(-64\pi^4\beta_i^2\gamma_j^2a^4b^4-16\pi^2\beta_i^4\gamma_j^2a^4a^6b^2\right. \\ &+ 16\pi^2\beta_i^2\gamma_j^4a^6b^2+4\beta_i^6\gamma_j^2a^8+6\beta_i^4\gamma_j^4a^8+4\beta_i^2\gamma_j^6a^8 \\ &- 256\pi^6b^6a^2\beta_i^2+96\pi^4b^4\beta_i^4a^4+96\pi^4b^4\gamma_j^4a^4 \\ &- 16\pi^2a^6b^2\beta_i^6+16\gamma_j^6\pi^2b^2a^6+\gamma_j^8a^8+\beta_i^8a^8 \\ &\left.+ 256\pi^8b^8+256\pi^6b^6\gamma_j^2a^2\right)^{-1},\end{aligned}$$

$$\begin{aligned}a_{ij}^{(8)} = {}& \frac{1}{2}\beta_j b^4 a_j^r w_j w_i a^4\gamma_i\left(16\pi^4b^4+24\gamma_i^2\pi^2b^2a^2\right. \\ &- 8\pi^2a^2b^2\beta_j^2+5\gamma_i^4a^4-10\gamma_i^2\beta_j^2a^4+\beta_j^4a^4\left.\right) \\ &\cdot\left(-64\pi^4\gamma_i^2\beta_j^2a^4b^4+16\pi^2\gamma_i^4\beta_j^2a^6b^2\right.\end{aligned}$$

$$
\begin{aligned}
&- 16\pi^2\gamma_i^2\beta_j^4a^6b^2 + 4\gamma_i^6\beta_j^2a^8 + 6\gamma_i^4\beta_j^4a^8 + 4\gamma_i^2\beta_j^6a^8 \\
&+ \beta_j^8a^8 + \gamma_i^8a^8 + 256\pi^6b^6\gamma_i^2a^2 - 256\pi^6b^6a^2\beta_j^2 \\
&+ 96\pi^4b^4\gamma_i^4a^4 + 96\pi^4b^4\beta_j^4a^4 + 16\gamma_i^6\pi^2b^2a^6 \\
&- 16\pi^2a^6b^2\beta_j^6 + 256\pi^8b^8\Big)^{-1},
\end{aligned}
$$

$$
\begin{aligned}
e_{ij}^{(8)} = {} & \frac{1}{2}\gamma_jb^4w_ja_i^rw_ia^4\beta_i\left(16\pi^4b^4 - 24\pi^2a^2b^2\beta_i^2\right. \\
&+ 8\gamma_j^2\pi^2b^2a^2 + 5\beta_i^4a^4 - 10\beta_i^2\gamma_j^2a^4 + \left.\gamma_j^4a^4\right) \\
&\cdot\left(-64\pi^4\beta_i^2\gamma_j^2a^4b^4 - 16\pi^2\beta_i^4\gamma_j^2a^6b^2\right. \\
&+ 16\pi^2\beta_i^2\gamma_j^4a^6b^2 + 4\beta_i^6\gamma_j^2a^8 + 6\beta_i^4\gamma_j^4a^8 + 4\beta_i^2\gamma_j^6a^8 \\
&- 256\pi^6b^6a^2\beta_i^2 + 256\pi^6b^6\gamma_j^2a^2 + \gamma_j^8a^8 \\
&+ 96\pi^4b^4\beta_i^4a^4 + 96\pi^4b^4\gamma_j^4a^4 - 16\pi^2a^6b^2\beta_i^6 \\
&+ \left.16\gamma_j^6\pi^2b^2a^6 + \beta_i^8a^8 + 256\pi^8b^8\right)^{-1},
\end{aligned}
$$

$$
a_{ij}^{(9)} = \frac{1}{2}\frac{w_iw_ja_i^ra_j^rb^4\beta_i^2\left(3\beta_j^2 + \beta_i^2\right)}{-3\beta_i^4\beta_j^2 + 3\beta_i^2\beta_j^4 + \beta_i^6 - \beta_j^6},
$$

$$
a_{ij}^{(10)} = -\frac{1}{2}\frac{w_iw_ja_i^ra_j^rb^4\beta_i\beta_j\left(3\beta_i^2 + \beta_j^2\right)}{-3\beta_i^4\beta_j^2 + 3\beta_i^2\beta_j^4 + \beta_i^6 - \beta_j^6},
$$

$$
\begin{aligned}
a_{ij}^{(11)} = {} & -\frac{1}{2}\beta_i^2a^4w_ia_i^rw_ja_j^rb^4\left(-24\pi^2a^2b^2\beta_j^2\right. \\
&+ 10\beta_i^2\beta_j^2a^4 + 5\beta_j^4a^4 + 16\pi^4b^4 - 8\pi^2a^2b^2\beta_i^2 \\
&+ \left.\beta_i^4a^4\right)\left(64\beta_i^2\beta_j^2\pi^4a^4b^4 + 16\beta_i^4\beta_j^2\pi^2a^6b^2\right. \\
&+ 16\beta_i^2\beta_j^4\pi^2a^6b^2 - 4\beta_i^6\beta_j^2a^8 + 6\beta_i^4\beta_j^4a^8 \\
&- 4\beta_i^2\beta_j^6a^8 - 256\pi^6b^6a^2\beta_i^2 - 256\pi^6b^6a^2\beta_j^2 \\
&+ 96\pi^4b^4\beta_i^4a^4 + 96\pi^4b^4\beta_j^4a^4 - 16\pi^2a^6b^2\beta_i^6 \\
&- \left.16\pi^2a^6b^2\beta_j^6 + \beta_j^8a^8 + \beta_i^8a^8 + 256\pi^8b^8\right)^{-1},
\end{aligned}
$$

$$
\begin{aligned}
a_{ij}^{(12)} = {} & -\frac{1}{2}\beta_i^2a^4w_ia_i^rw_ja_j^rb^4\left(-24\pi^2a^2b^2\beta_j^2\right. \\
&+ 10\beta_i^2\beta_j^2a^4 + 5\beta_j^4a^4 + 16\pi^4b^4 - 8\pi^2a^2b^2\beta_i^2 \\
&+ \left.\beta_i^4a^4\right)\left(64\beta_i^2\beta_j^2\pi^4a^4b^4 + 16\beta_i^4\beta_j^2\pi^2a^6b^2\right. \\
&+ 16\beta_i^2\beta_j^4\pi^2a^6b^2 - 4\beta_i^6\beta_j^2a^8 + 6\beta_i^4\beta_j^4a^8 \\
&- 4\beta_i^2\beta_j^6a^8 - 256\pi^6b^6a^2\beta_i^2 - 256\pi^6b^6a^2\beta_j^2 \\
&+ 96\pi^4b^4\beta_i^4a^4 + 96\pi^4b^4\beta_j^4a^4 - 16\pi^2a^6b^2\beta_i^6 \\
&- \left.16\pi^2a^6b^2\beta_j^6 + \beta_j^8a^8 + \beta_i^8a^8 + 256\pi^8b^8\right)^{-1},
\end{aligned}
$$

$$
\begin{aligned}
a^{(13)} = {} & \gamma_i\beta_ia^2w_i^2\pi^2a_i^rb^2\left(-16\pi^2a^2b^2\beta_i^2 - 10\gamma_i^2\beta_i^2a^4\right. \\
&+ 3\beta_i^4a^4 + 16\pi^2\gamma_i^2b^2a^2 + 3\gamma_i^4a^4 + \left.16\pi^4b^4\right)\left(\beta_i^8a^8\right. \\
&+ 96\pi^4b^4\beta_i^4a^4 - 16\pi^2a^6b^2\beta_i^6 + 96\pi^4b^4\gamma_i^4a^4 \\
&+ 16\gamma_i^6\pi^2b^2a^6 + 256\pi^6b^6\gamma_i^2a^2 - 256\pi^6b^6\beta_i^2a^2 \\
&+ 6\gamma_i^4\beta_i^4a^8 + 4\gamma_i^2\beta_i^6a^8 + 4\gamma_i^6\beta_i^2a^8 + 256\pi^8b^8 \\
&+ \gamma_i^8a^8 - 64\gamma_i^2\beta_i^2a^4\pi^4b^4 + 16\gamma_i^4\beta_i^2a^6\pi^2b^2 \\
&- \left.16\gamma_i^2\beta_i^4a^6\pi^2b^2\right)^{-1},
\end{aligned}
$$

$$
\begin{aligned}
b^{(13)} = {} & a^2w_i^2\pi^2a_i^rb^2\left(16\pi^4b^4\beta_i^2 - 16\pi^4b^4\gamma_i^2\right. \\
&- 8\pi^2b^2\gamma_i^4a^2 - 8\pi^2b^2\beta_i^4a^2 + 48\pi^2b^2\gamma_i^2\beta_i^2a^2 \\
&- 15\gamma_i^2\beta_i^4a^4 + \beta_i^6a^4 - \gamma_i^6a^4 + 15\gamma_i^4\beta_i^2a^4\left.\right)\left(\beta_i^8a^8\right. \\
&+ 96\pi^4b^4\beta_i^4a^4 - 16\pi^2a^6b^2\beta_i^6 + 96\pi^4b^4\gamma_i^4a^4 \\
&+ 16\gamma_i^6\pi^2b^2a^6 + 256\pi^6b^6\gamma_i^2a^2 - 256\pi^6b^6\beta_i^2a^2 \\
&+ 6\gamma_i^4\beta_i^4a^8 + 4\gamma_i^2\beta_i^6a^8 + 4\gamma_i^6\beta_i^2a^8 + 256\pi^8b^8 \\
&+ \gamma_i^8a^8 - 64\gamma_i^2\beta_i^2a^4\pi^4b^4 + 16\gamma_i^4\beta_i^2a^6\pi^2b^2 \\
&- \left.16\gamma_i^2\beta_i^4a^6\pi^2b^2\right)^{-1},
\end{aligned}
$$

$$
c^{(13)} = -\frac{w_i^2\pi^2a_i^r\beta_i\gamma_ib^2}{\left(\beta_i^4 + 2\gamma_i^2\beta_i^2 + \gamma_i^4\right)a^2},
$$

$$
d^{(13)} = \frac{1}{2}\frac{w_i^2\pi^2a_i^r\left(\beta_i^2 - \gamma_i^2\right)b^2}{\left(\beta_i^4 + 2\gamma_i^2\beta_i^2 + \gamma_i^4\right)a^2},
$$

$$
e^{(13)} = \frac{1}{32}\frac{w_i^2\left(a_i^{r2}\beta_i^2 + \gamma_i^2\right)a^2}{\pi^2b^2},
$$

$$
f^{(13)} = \frac{1}{32}\frac{w_i^2\pi^2b^2}{a^2\gamma_i^2},
$$

$$
g^{(13)} = \frac{1}{32}\frac{w_i^2\pi^2a_i^{r2}b^2}{a^2\beta_i^2}.
\tag{A.2}
$$

The coefficients given in (18a) and (18b) can be expressed as

$$
A_1 = \frac{2w_1w_2a^2b^2\left(91a^4 + 80a^2b^2 + 16b^4\right)}{81a^8 + 720a^6b^2 + 1888a^4b^4 + 1280a^2b^6 + 256b^8},
$$

$$
A_2 = \frac{1}{2}\frac{w_1w_2a^2b^2\left(365a^4 + 328a^2b^2 + 80b^4\right)}{81a^8 + 720a^6b^2 + 1888a^4b^4 + 1280a^2b^6 + 256b^8},
$$

$$
B_1 = \frac{3}{16}\frac{w_1w_3a^2b^2\left(21a^4 + 10a^2b^2 + b^4\right)}{16a^8 + 40a^6b^2 + 33a^4b^4 + 10a^2b^6 + b^8},
$$

$$B_2 = \frac{1}{16}\frac{w_1 w_3 b^2\left(65a^4 + 34a^2b^2 + 5b^4\right)}{16a^8 + 40a^6b^2 + 33a^4b^4 + 10a^2b^6 + b^8},$$

$$C_1 = \frac{6w_2 w_3 a^2 b^2\left(651a^4 + 208a^2b^2 + 16b^4\right)}{625a^8 + 5200a^6b^2 + 11616a^4b^4 + 3328a^2b^6 + 256b^8},$$

$$C_2 = \frac{1}{2}\frac{w_2 w_3 a^2 b^2\left(7813a^4 + 2504a^2b^2 + 208b^4\right)}{625a^8 + 5200a^6b^2 + 11616a^4b^4 + 3328a^2b^6 + 256b^8},$$

$$A_3 = -\frac{2}{9}\frac{w_1 w_2 b^2}{a^2},$$

$$A_4 = -\frac{5}{18}\frac{w_1 w_2 b^2}{a^2},$$

$$B_3 = -\frac{3}{64}\frac{w_1 w_3 b^2}{a^2},$$

$$B_4 = -\frac{5}{64}\frac{w_1 w_3 b^2}{a^2},$$

$$C_3 = -\frac{6}{25}\frac{w_2 w_3 b^2}{a^2},$$

$$C_4 = -\frac{13}{50}\frac{w_2 w_3 b^2}{a^2},$$

$$A_5 = \frac{1}{16}\frac{w_1^2 b^2}{a^2},$$

$$A_6 = \frac{1}{64}\frac{w_2^2 b^2}{a^2},$$

$$A_7 = \frac{1}{144}\frac{w_3^2 b^2}{a^2},$$

$$W_c = \frac{1}{32}\frac{a^2\left(w_1^2 + 4w_2^2 + 9w_3^2\right)}{b^2}. \tag{A.3}$$

Competing Interests

The authors declare that there is no conflict of interests regarding the publication of this article.

Acknowledgments

The authors gratefully acknowledge the National Natural Science Foundation of China (NNSFC) through Grant nos. 11172011 and 11472019.

References

[1] A. D. Dimarogonas, "Vibration of cracked structures: a state of the art review," *Engineering Fracture Mechanics*, vol. 55, no. 5, pp. 831–857, 1996.

[2] J. R. Rice and N. Levy, "The part-through surface crack in an elastic plate," *Journal of Applied Mechanics*, vol. 3, pp. 183–194, 1972.

[3] H. P. Lee, S. P. Lim, and S. T. Chow, "Prediction of natural frequencies of cracked isotropic and orthotropic composite plate," in *Proceedings of the International Conference on Computational Engineering Mechanics*, pp. 632–648, Beijing, China, 1987.

[4] S. E. Khadem and M. Rezaee, "An analytical approach for obtaining the location and depth of an all-over part-through crack on externally in-plane loaded using vibration analysis," *Journal of Sound and Vibration*, vol. 230, pp. 291–308, 1999.

[5] S. E. Khadem and M. Rezaee, "Introduction of modified comparison functions for vibration analysis of a rectangular cracked plate," *Journal of Sound and Vibration*, vol. 236, no. 2, pp. 245–258, 2000.

[6] Sh. Hosseini-Hashemi, Gh. Heydar Roohi, and D. T. HosseinRokni, "Exact free vibration study of rectangular Mindlin plates with all-over part-through open cracks," *Computers and Structures*, vol. 88, no. 17-18, pp. 1015–1032, 2010.

[7] Y. Fu, Y. Xiao, and X. Zha, "Nonlinear vibration for moderate thickness rectangular cracked plates including coupled effect of elastic foundation," *Applied Mathematics and Mechanics*, vol. 8, no. 26, pp. 963–972, 2005.

[8] A. Israr and L. Atepor, "Investigation of the nonlinear dynamics of a partially cracked plate," in *Proceedings of the 7th International Conference on Modern Practice in Stress and Vibration Analysis*, vol. 181, 2009.

[9] J. Yang, Y. X. Hao, W. Zhang, and S. Kitipornchai, "Nonlinear dynamic response of a functionally graded plate with a through-width surface crack," *Nonlinear Dynamics*, vol. 59, no. 1-2, pp. 207–219, 2010.

[10] A. Saito, M. P. Castanier, and C. Pierre, "Estimation and veering analysis of nonlinear resonant frequencies of cracked plates," *Journal of Sound and Vibration*, vol. 326, no. 3–5, pp. 725–739, 2009.

[11] R. Ismail and M. P. Cartmell, "An investigation into the vibration analysis of a plate with a surface crack of variable angular orientation," *Journal of Sound and Vibration*, vol. 331, no. 12, pp. 2929–2948, 2012.

[12] T. Bose and A. R. Mohanty, "Vibration analysis of a rectangular thin isotropic plate with a part-through surface crack of arbitrary orientation and position," *Journal of Sound and Vibration*, vol. 332, no. 26, pp. 7123–7141, 2013.

[13] H. AsadiGorgi, M. Dardel, and M. H. Pashaei, "Effects of all-over part-through cracks on the aeroelastic characteristics of rectangular panels," *Applied Mathematical Modelling*, vol. 39, no. 23-24, pp. 7513–7536, 2015.

[14] M.-H. H. Shen and Y. C. Chu, "Vibrations of beams with a fatigue crack," *Computers and Structures*, vol. 45, no. 1, pp. 79–93, 1992.

[15] N. Pugno, C. Surace, and R. Ruotolo, "Evaluation of the non-linear dynamic response to harmonic excitation of a beam with several breathing cracks," *Journal of Sound and Vibration*, vol. 235, no. 5, pp. 749–762, 2000.

[16] S. Caddemi, I. Caliò, and M. Marletta, "The non-linear dynamic response of the Euler-Bernoulli beam with an arbitrary number of switching cracks," *International Journal of Non-Linear Mechanics*, vol. 45, no. 7, pp. 714–726, 2010.

[17] F. E. Dotti, V. H. Cortinez, and F. Reguera, "Non-linear dynamic response to simple harmonic excitation of a thin-walled beam with a breathing crack," *Applied Mathematical Modelling*, vol. 40, no. 1, pp. 451–467, 2016.

[18] J. N. Reddy, *Mechanics of Laminated Composite Plates and Shells: Theory and Analysis*, CRC Press, Boca Raton, Fla, USA, 2nd edition, 2004.

[19] G. Z. Harris, "The buckling and post-buckling behaviour of composite plates under biaxial loading," *International Journal of Mechanical Sciences*, vol. 17, no. 3, pp. 187–202, 1975.